Particle Movement in Paper Porous Media: Influence Factors and Model

By
Huan Hsuan Hsu, M.S

A Thesis
Submitted to the School of Graduate Studies
In Partial Fulfillment of the Requirements
For the Degree
Master of Applied Science

McMaster University

Particle Movement in Paper Porous Media: Influence Factors and Model

Master of Applied Science (2010) Chemical Engineering

McMaster University Hamilton, Ontario

TITLE: Particle Movement in Paper Porous Media: Influence Factors and Model

AUTHOR: Huan Hsuan Hsu

M.S. (National Chang Kung University, Taiwan)

SUPERVISOR: Professor Robert H. Pelton

NUMBER OF PAGERS: X, 87

ABSTRACT

In recent years, paper-based analytical devices have been widely applied in many areas such as chemical analysis, disease diagnosis, and contaminant sensing. From the most common utility in pH paper to novel electrochemical sensing devices for monitoring heavy metals or glucose (*2*), paper-based analytical devices have shown great potential to become alternative analytical technologies. In paper based analytical device, commonly, the samples are transport by the capillary force from enter site toward the testing area. However, there is still not enough information of sample transportation in paper. This research focused on understanding the particle movement during elution in paper in order to provide some useful information for design and manufacture of paper analytical devices.

There are many factors that influence the particle movement in paper, such as particle properties (i.e. surface potentials), paper properties (i.e. salt content on paper) and ambient factors (i.e. humidity). The effects of those factors on particle movement in paper were studied by the elution experiments. The elution experiments were conducted by vertically dipping the bottom 1 cm of paper strips (Whatman No. 1) into polystyrene latex solutions. The latex solutions were eluted up by the capillary force of paper, which was spontaneously occurred due to the porous structure of paper. Then, by varying the testing factors, respectively, the effects caused by those factors can be investigated.

Since paper is composed of cellulose with many carboxyl groups, it is negatively charged. Therefore, the surface potential of particles was considered as an important factor that influences particle movement and deposition. More deposition was observed when particles with more positive charge were eluted in paper and vice versa. In addition, the influence of the flow velocity on particle movement during elution was also studied. The flow velocity was varied by changing the shape of paper strips. No obvious influence of the flow velocity on anionic particle deposition was observed, while the raise of the flow velocity increased cationic particle deposition. Moreover, the particle (cationic and anionic) deposition was increased when latexes flowed through paper strips with salt content. The salt was dissolved once it contacted by the elution flow, which resulted in the increase of ionic strength in the elution flow. As a result, increased particle deposition were observed due to the reduced electrical double layer repulsive forces (particle-particle and anionic particle-paper surface) caused by increased ionic strength.

Nevertheless, in all the experiments described before, it was noted that there was always a band shape of concentrated particles at the elution end (where elution flow stopped flowing forward). This phenomenon was caused by the mass flow (MF_E), which occurred in order to refill the water loss due to evaporation. After the capillary flow reached the elution end, the suspended particles were carried continuously up to the elution end by MF_E and concentrated gradually. To describe the movement of this evaporation-driven flow, the model suggested by Fries (*29*) (Eq. 4.2.11) was applied. The results predicted from this model fitted the experimental data well. The influences of evaporation on elution flow movement were further investigated based on this model. The effects of paper properties on the maximum elution distance were also examined based on the model of Fries (*29*) (Eq. 4.2.11). The results showed the influences of paper properties were in the order as: pore radius (capillary radius (Rs)) > permeability (K) $\fallingdotseq$ thickness (δ) > contact angle (θs) >> porosity (ϕ) (no effect).

ACKNOWLEDGEMENT

In the first place, I would like to express my deep appreciation to my supervisor, Professor Dr. Robert H. Pelton for his instruction during the whole period of my research.

I would like to thank my supervisor Professor Dr. Carlos Filipe for many treasurable advises during setting up my model. I would like to thank Mr. Doug Keller and Ms. Sally Watson for their assistance with my research.

I am grateful to all my colleagues in Interfacial Science and Technologies Group at McMaster: Dr. Yuguo Cui, Dr. Anil Khanal, Dr. Wei Chen, Roger Ren, Liang Zhang, Songtao Yang, Ruilin Li, Dan Zhang, Zuohe Wang, Yaqin Xu, Quan Wen, Jingyun Wang, Vincent Leung and Behnam Naderi Zand. Special thanks to Roger Ren for lots of fruitful discussion about my experiment data.

I would like to thank my father 徐清棋 先生and my mother 張玉美 女士 for their understanding and support of my life in Canada. Special thanks to my wife Allison Yeh for her supports every moment during my Master study life.

Finally, I would like to thank Sentinel Network and NSERC for the financial support.

TABLE OF CONTENT

LIST OF FIGURES

LIST OF TABLES

Chapter One: Introduction

1.1 Paper based analytical device

1.1.1 Paper structure

Paper is a continuous porous medium mainly composed of cellulose fibers. According to the definition in William Clark Bliesner's Ph.D thesis (1): paper is a compressible and anisotropic porous medium. Paper is compressible so that the bulk dimension of paper can be changed by the application of an external force. Paper is also anisotropic since cellulose fibers generally lie with their axes preferentially in the plate of sheet (which named mechanical direction)(*1*), which causes different permeabilities and penetration velocities in the mechanical and cross section directions. Back studied the spreading behaviour of a fluid drop onto paper sheets and he found that the capillary penetration velocity for most papers is 5-15% larger in the machine direction than that in the cross section direction (*2*). Similarly, Horstmann *et al.* tested the permeabilities of Fourdrinier neutral sized bleached kraft paper in both directions and suggested that the machine direction permeability is about 20% higher than the cross-direction permeability (*2*).

There are some channels existing in paper network structure which made the flow and penetration of fluids (gases or liquids) through paper possible. These channels, connecting pores of various sizes and shapes, are branched or interconnected to form paper as a whole. Thus, it is difficult to measure a definite dimension which is characteristic of a particular pore space (*1*). As a result of this structure, the pore size or pore size distribution of paper porous media can only be defined by experimental techniques (i.e. mercury intrusion) and model approach.

1.1.2 Paper analytical device

The first paper-based analytical device was invented during the early 20th century also known as paper chromatography. In the mean time, scientists started developing diagnostic and bio-detection devices on paper strips (*3*). Until now, paper based analytical devices are widely used in chemical analyses, disease diagnoses, and contaminant sensing. From the most common utility in pH paper to novel electrochemical sensors for monitoring heavy metals or glucose (*4*), paper based analytical devices show great potential to become alternative analytical technologies. In the next paragraphs, some significant developments are introduced.

Paper is a thin material typically composed of cellulose fibers. Researchers focused on paper based analytical devices for many advantages (*5, 6*): (i) paper is a widely used and an inexpensive material (*3*). Therefore, most of paper-based devices can be fabricated at low cost. (ii) Paper is thin, light-weight (~ 100 g/m^2), available in a wide range of thicknesses (0.07-1 mm), and is also easy to stack, store, and transport. (iii) The porous structure of paper provides spontaneous capillary flow energy for transporting samples without active pumping. (iv) Paper is bio-friendly and compatible with many bio-samples. (v) Paper is biodegradable and easily burned. Therefore, paper based devices can be easily disposed of, after dealing with hazardous samples. (vi) There are many well-developed surface modification technologies of paper such as printing, coating, surface grafting and sizing which facilitate application of paper in multi target samples.

Recently, Whitesides and coworkers (3) invented a novel analytical strategy by patterning hydrophobic barriers on paper to form the micro channel device. By applying this device, multiplex analysis can be achieved with promising sensitivity and only a small amount of samples are required. In detail, this device works by printing patterns on paper with Polydimethylsiloxane (PDMS) "ink" (7) or patterned paper by photo resist lithography (8) to form hydrophobic boundaries to direct fluids to the test area.

Later on, Lu *et al.* (*9*) presented another simple and low cost method to produce paper-based micro channel device by using a wax printer to print designed wax micro channel patterns on paper. Also, Abe *et al.* (*10*) introduced a new inkjet printing technology by etching polystyrene film pre-coated on paper with toluene to fabricate micro channels on paper.

The first multiplex analysis by using paper-based micro fluidic devices was for urinalysis created by Whitesides and coworkers (*11*). They prepared micro fluidic devices with one inlet and three branched test zones by photo resist lithography. The urine samples were dipped in the inlet zone and carried to three separate test zones by paper capillary forces. Two well-known chemical reactions were introduced in the test zone to test glucose and protein in the urine samples (potassium iodide and 1:5 horseradish peroxidase/glucose oxidase solution for the glucose assay, tetrabromophenol blue (TBPB) in pH 1.8 buffer for the protein assay). Furthermore, by colorimetric method, the quantitative detection is also achieved. In their later work, Whitesides and coworkers applied imaging devices (camera phone or portable scanner) for more precise quantitative analysis (*12*). In detail, all assay results with different colour intensities were first recorded by an imaging device. These digital images were then transferred to an off-site laboratory for analysis by instruments with higher sensitivity and well-trained technicians. For the last step, the final analytical results were transferred back to the in-field testers. More recently, Whitesides' group created paper micro zone plates to make 96, 384 or even more working colorimetric assays in one device (*13*). Also, they invented 3D micro channel devices by assembling multilayer paper with channels patterned in one device which is anticipated to make compact devices with more functions (*14*). Figure 1.1 shows all the works Whitesides' group have achieved.

In comparison, Sentinel network lead by Dr. Pelton devotes their research to bioactive paper and makes significant contributions in this area. By introducing different immobilization strategies, they successfully placed bio-sensors on paper strips to prepare a bio-active paper device sensitive to selected pathogens (*5*).

Su and coworkers successfully immobilized DNA aptamers and antibodies by applying carboxylated Poly(*N*-isopropylacrylamide) (PNIPAM) microgels as carriers. The biomolecules were covalently coupled with microgels as "ink," then coated on paper by inkjet printing. The PNIPAM coupled biomolecules showed great immobilization results, and the biological functions of those biomolecules were also well maintained (*15*).

Gold nanoparticles (AuNP) are known to have unique color properties; AuNP shows red or blue depending on its dispersed or aggregated state, respectively. By applying AuNP, Zhao *et al.* invented a paper based colorimetric bio-sensor for detecting DNase I (*16*). In detail, AuNP was first aggregated by hybridizing with interparticle DNA, and then coated on paper. Once DNase I appeared on this array area, this enzyme would break double-stranded DNA cross links leading to the dispersion of AuNP aggregation (consequently the color would change from blue to red). Furthermore, this AuNP paper based bio-sensor is able to keep its biological functions, even after it has been oven-dried and put in long term storage.

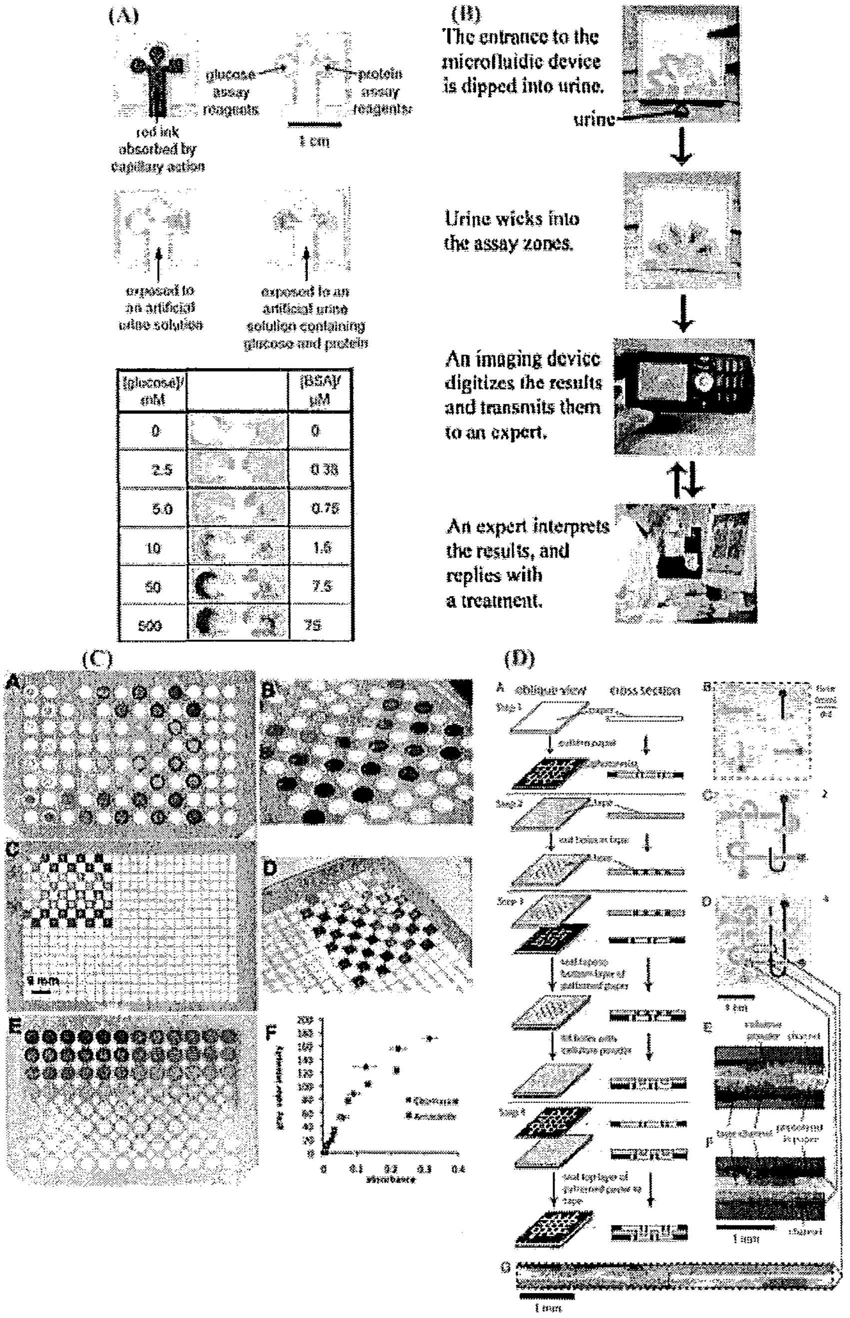

Figure 1.1 Typical paper micro fluidic devices: (A) First paper micro fluidic device for urinalysis, (B) Applied image device for off-site analysis, (C) paper micro zone plates for multi colorimetric assays, (D) 3D paper micro fluidic device (*3*, *6*)

Wang *et al.* (*17*) worked on the compatibility of antibodies and wet-strength paper. They found that the activity of antibodies was still maintained after being coated on polyamide-epichlorohydrin (PAE) or Polyvinylamine (PVAm) pretreated paper. Therefore, wet-strength paper is a suitable support for antibody assays. Moreover, after testing the activity of antibodies coated on different substrates, the results demonstrated that cellulosic filters show better compatibility with antibodies than that of glass fibers or synthetic fiber filters.

However, even with many applications of paper-based analytical devices, sufficient fundamental research is lacking with regards to particle transported through paper media and factors that influence the transportation phenomenon such as paper properties and particle properties (i.e. surface charge, ionic strength etc) as well as environmental conditions (i.e. relative humidity, temperature). Therefore, this research is focused on understanding how and why these factors influence sample transportation.

1.2 Water penetration in paper

Water is the most common carrier for sample transportation in paper media. In order to study the transportation of samples in paper, the understanding of water transportation in paper is necessary. The phenomenon of liquid capillary penetration into paper appears in many researches and industry processes such as paper chromatography, printing, reprographic, and textile technology (*18*). Nissan suggested that water transport through paper porous media can be divided into four different mechanisms (*19*):

1. water penetration through the pores of paper by the capillary flow
2. water moves through the pores of paper by the surface diffusion
3. water moves through paper fibers
4. water vapor moves through pores of paper

Several models have been proposed to study the phenomenon of liquids spreading and penetrating porous structures (e.g. paper, cotton fiber and yarns). The capillary model, which is fundamentally based on the equation to describe capillary penetration, was presented by Lucas and Washburn in the early 19th century (*20*):

$$H(t) = \left(\frac{\gamma_{LV} R \cos\theta}{2\eta}\right)^{1/2} \sqrt{t} \qquad \text{Eq 1.2.1}$$

Where γ_{LV} is the surface tension of the liquid, η is the shear viscosity, R is the pore radius, and θ is the contact angle between the liquid and the capillary media. Based on this equation, the liquid penetration distance is thus proportional to the square root of time. In addition, Lucas-Washburn's equation is based on the assumptions that all the capillaries have the same diameter and those capillaries do not connect to each other. Also, the length of the capillaries must be greater than their diameters. These assumptions do not exactly fit the paper structure (*21*). Furthermore, the equation is adequate for non-aqueous liquids which do not swell paper fibers (*22*). Its applicability to the penetration of water-based liquids such as printing inks leaves much to be desired (*19*). Thus, many researches have conducted to compensate for these deficiencies.

Marmur (*23, 24*) suggested the radial capillary model for further refinement in modeling liquid penetration in porous media particularly in paper structures. This model is based on the thermodynamics and the Lucas-Washburn kinetics of radial penetration between two parallel discs. Two limiting cases are presented with respect to the hysteresis of the contact angle which the liquid drop makes with the outside surface of the plate: (a) no hysteresis and (b) constant radius (Fig 1.2). The experimental results shows that the penetration into a radial capillary rarely occurs when the contact angle is larger than 90 °, due to the effect of hysteresis.

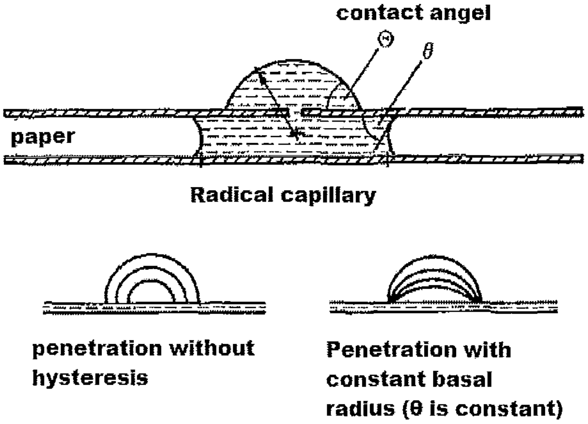

Figure 1.2 Radial capillary and two limiting cases (*23*)

The research of Borhan and Rungta (*25*) focused on the capillary penetration of aqueous liquid systems into various papers. The penetration kinetics of radial penetration in an infinite liquid reservoir is well described by Marmur's model.

Moreover, in the nano scale tube capillary raise simulation conducted by Dimitrov *et al* (*26*), Lucas Washburn's equation agrees well with the simulation and experimental results of the nano scale capillary flow, but just needs a simple modification when the scale is small enough that the slip flow cannot be neglected.

Evaporation is another important factor that influences the water movement during water penetration in paper. Lockington *et al.* (*27*) proposed a model to describe the phenomenon of moisture wicking (liquid penetration by capillary eluting) in a paper sheet. This model is based on a nonlinear diffusion equation of moisture content plus a linear term accounting for the evaporation rate which is associated with the moisture content in paper. With the presence of the evaporation factor in the model, the numerical results of the characteristics of wicking in paper such as the wetting front and the uptake rate matched well with the experimental data. Moreover, the results of Lockington's work (*27*) suggests that the uptake rate of water in paper is proportional to the square root of the evaporation coefficient. Also, the maximum wicking distance is inversely proportional to the square root of evaporation coefficient. The evaporation coefficient is the ratio of the real evaporation rate with the theoretical maximum evaporation rate, which depends on several ambient environmental factors such as humidity and pressure (*28*).

In their recent work, Fries *et al.* (*29, 30*) applied the Lacus-Washburn equation to describe the phenomenon of water upward movement by the capillary force in hanging (vertical) porous sheets (metallic weave). The experimental results showed good agreement with the Lacus-Washburn equation in those flow regions where the effects of gravity and evaporation were negligible. In addition, Fries *et al*, found that the capillary flow rates were about two times faster in the vertical direction than that in the horizontal direction, which was due to the evaporation. Evaporation also showed significant influence on the maximum wicking distance. Therefore, a model based on the mass balance was developed to describe the evaporation effect on the capillary rise of water in porous media. In this model, a refill flow for replenishing losses of liquid due to the evaporation was suggested to occur at all times during wicking. The results of the experiments conducted with various fluids and evaporation rates showed good agreement with this model. Nevertheless, the result of the maximum wicking distance predicted by the model was 20% higher than the experimental data. This is explained by Fries *et al.* that the evaporation rate in their model was assumed constant. However, the evaporation rate on the wicking top may be higher which would lead to this discrepancy between the experimental data and modeling simulation (*29*).

1.3 Particle transport in porous media: mechanisms and influence factors

Colloid transport in porous media has been broadly investigated in many research areas. Most research is based on environmental subjects such as the transportation of colloid-facilitated contaminants and bio colloids (viruses and bacteria) in groundwater and the subsurface soil (*31, 32*). By those studies, the colloid transport mechanisms were well investigated. Some researches further modeled the spreading of contaminants and bio-colloids in natural porous media. Those researches were well summarized in DeNovio's review (*33*). In the area of colloid transport, the entrapment of particles by porous media (filter out particles from water flow) always attracts the most interest and attention. In Sen's (*34*) review article, three main mechanisms of entrapment have been demonstrated: size exclusion, multi-particle bridging, and surface deposition. The details are conceptually shown in Fig 1.3.

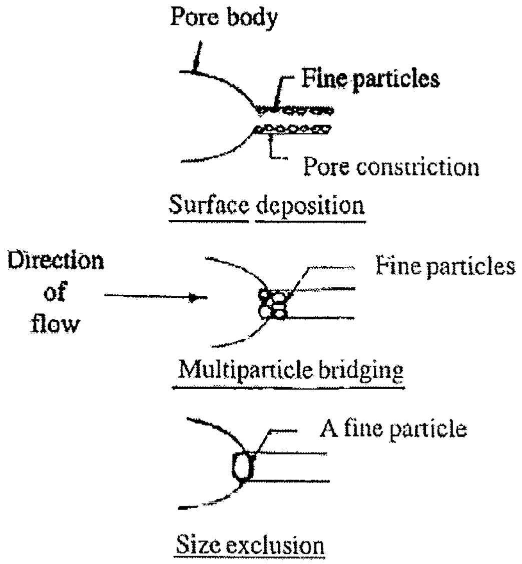

Figure 1.3 Concept of particle entrapment in porous media Figure from Ref (*34*).

If the size of the colloid particle is equal to or greater than the pore size, the entrapment and pore plugging would definitely take place. However, in the real environment, both colloids and pores have random size distributions. Herzig *et al.* found that the main factor determining the mechanism of colloid entrapment was the ratio of colloid particle size over pore size (SR value) (*35*). Table 1.1 shows the qualitative results for the entrapment mechanisms of filtration at different particle size/pore size ratio (SR values) (*36*). Single particle entrapment occurs when the particle size is bigger or equal to the pore size (SR $\geqq 1$). Once the SR value is within 0.6 to 0.04, multi particle blocking may occur. Multi particle blocking is influenced by the pore constriction and the colloid flow velocity. Pandya et al. (*37*) suggested that once the concentration of the colloid was higher than a critical particle concentration (CPC), the pore would be plugged by multiple particles, preventing the colloid from flowing through.

Table 1.1 Mechanisms of particle entrapment determined by ratio of particle size / pore size (SR value)

SR value	Applicable entrapment mechanisms
$\geqq 1$	blocking or size exclusion
0.1 to 0.6	bridging and multi particle blocking
0.04 to 0.1	surface deposition, bridging and multi particle blocking
0.01 to 0.04	surface deposition

Retention of particles caused by surface deposition takes place when SR values are within 0.1 to 0.01. Once the SR values is lower than 0.04, particle deposition would become the main mechanism of particle entrapment. In the last decade, in order to understand the phenomenon of small (micro or nano) particles travelling in porous media, many researches have been conducted to analyze particle deposition on porous media surface (*38*). For small particles travelling in porous media, DLVO theory is usually applied to describe particle movement while flowing through porous media.

1.3.1 DLVO theory in particle transport in porous media

When colloid particles are transported in porous media, there are two interactions determining the trajectory of particle movement: (1) van der Waals interaction (V_A) and (2) the electrical double layer interaction (V_R) (*39*). DLVO theory predicts the particle movement by calculating the net potential of V_A (generally attractive) and V_R (repulsive if the surface charge of the particles and porous media are homogeneous) between particles and the porous surface. Fig 1.4 shows the theoretical scheme of DLVO theory.

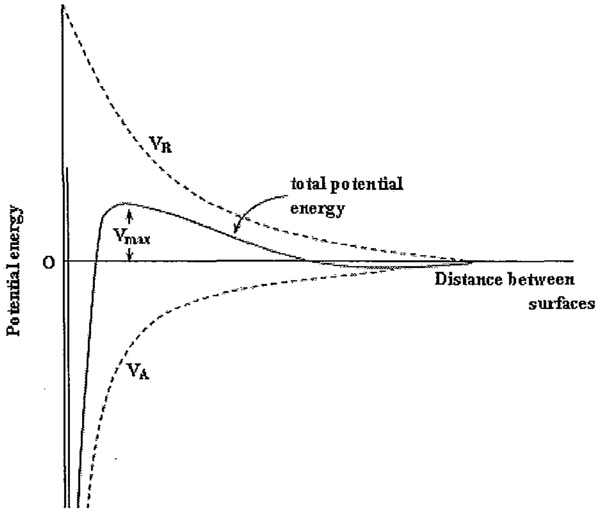

Figure 1.4 The theoretical scheme of DLVO theory, adapted from ref (*40*)

In short, during latex flow through porous media, particles are first attracted by van der Waal forces and move towards the porous media surface. Once the distances between particles and porous media surface decrease to a specific range, the effect of V_R would become more significant and generate an energy barrier to prevent further approach of particles. If the particles are able to overcome the energy barrier, V_A would dominate again and cause the particles deposition on the porous media surface.

Early research showed that many factors can influence the DLVO interactions between porous surfaces and flowing particles, such as the ionic strength and pH in latex solution (*41*), surface properties of latex particles (*42*), the surface roughness and structures of the porous media (*43*). The thickness of the electrical double layer is inversely proportional to the square root of the ionic strength. As the ionic strength decreases, the thickness of electrical double layer increases which enhances electrical interaction (V_R)) and amplifies the energy barrier. Colloids have to overcome the barrier to enter the secondary minimum where colloid is able to deposit onto substrate surfaces. Consequently, we can predict that less deposition would be observed in the system with lower ionic strength under unfavorable deposition conditions (homogeneous surface charge of colloids and substrates) (*44, 45*). On the contrary, increasing the ionic strength decreases the thickness of the double layer (*46, 47*), and the secondary minimum would shift closer to the media surface. Therefore, colloids are able to reach a position close enough to substrate surfaces where van der Waals would dominate the particle movement. Several studies of colloids flowing through porous media show that the high ionic strength in colloid solutions reduces the electrical repulsive force, and thus enhances colloid deposition on porous media surfaces (*48, 49*).

If the surface charges of latex and porous media surface are heterogeneous, the electrical interaction would act attractively. Therefore, the energy barrier between the particle and the porous media surface no longer exists. Once particles reach the working distance of V_A, particles would be attracted to deposit on substrates. However, the particle deposition is also restricted in this circumstance. This restriction of deposition is attributed to the repulsive force between the deposited particles and the suspended particles in the subsequent liquid flowing through. This surface exclusion phenomenon is called **blocking** (*50, 51*). Blocking usually takes place during stable latex transport in porous media. A monolayer of particles is assumed to be the maximum deposition amount on porous media surface once blocking effect occurs. In the research of Liu *et al.* (*32*), the blocking effect was observed in transportation of aluminum oxide particles (cationic) in anionic porous media. The influence of ionic strengths on blocking was also studied in this research (*32*); as shown in Fig 1.5, C/Co in this figure represents the ratio between outlet and inlet particle concentration (for example, C/Co = 1 means no deposition occurs during transportation). In the control experiment that colloids were suspended in deionized water, the deposition rate was reduced significantly while the blocking effect was dominant. However, increasing the ionic strength retarded the blocking effect. Liu *et al.* (*32*) suggested the retardation of the blocking effect is due to the reduction of repulsive particle-particle electrical forces as the ionic strength increased. Consequently, we can make a conclusion that once the **ionic strength** increases in the system, more particles would deposit regardless of repulsive or attractive colloid-substrate interactions.

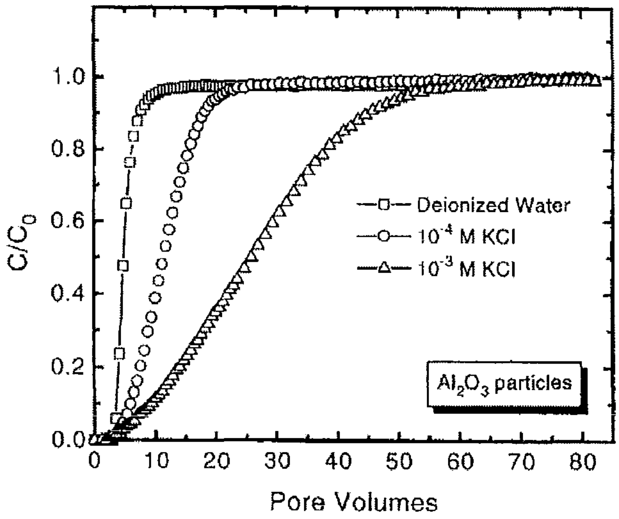

Figure 1.5 Particle breakthrough curves for colloidal alumina depositing onto anionic substrate. The curves showed different ionic strengths and C/Co values. The results demonstrated the effect of ionic strength on the rate of blocking (*32*).

Many studies suggest that flow velocity causes significant influence on colloid deposition and transportation. For example, Smith *et al.* (*52*) found that bio-colloid deposition rate in soil was inversely proportional to water flow velocity. Huysman *et al.* (*53*) also observed that colloid flow in filter was more efficient when a higher flow velocity was applied. Sharma *et al.* (*54*) suggested that the raise of flow velocity increases the distance shorten the contact time between the colloids and substrates; hence, the colloid deposition was decreased. Moreover, later research done by Bhagat (*55*) also showed that in micro channel filtration systems, the decreasing of flow velocity (lower Reynolds number) enhanced the filtration efficiency. Research conducted by Muller (*56*) presented that the capillary flow velocity on paper strips can be controlled by paper strip shapes. He suggested that restricting the paper channel radius leaded to an acceleration of flow velocity.

1.3.2 The deposition of cationic particles onto anionic paper fiber surface

In 70s to 80s, Alince *et al. (57-62)* conducted a series experiment to investigate the mechanisms of colloid particle deposition on anionic paper fibers. Based on their experimental results, they suggested: (1) anionic particles were hardly deposited on anionic fibers because of the charge repulsing effect; (2) The deposition amounts of cationic colloids would reach a plateau. Particle deposition amounts of that level were similar to amounts of a monolayer of latex particles which fiber surfaces can accommodate (3) cationic particle deposition increased with the raise of salt content in the circumstance that the hydrodynamic effects was not strong enough to influence the particle aggregation; (4) the particle deposition retarded the liquid penetration in paper.

1.4 Particle concentrated on the liquid-substrate contact line

In the experimental results of Deegan's group, it can be observed that the contact line between the liquid drop and the substrate remains pinned during most of the drying processes. Moreover, the highest evaporation rate takes place at the drop's edge and more liquid is concentrated near the center of the drop. Once the liquid at the drop's edge evaporates, in order to keep the contact line pinned, an outward flow has to occur inside the drop to replenish the loss of liquid at the drop edge. This flow also transports the suspended solute to the contact line and consequently, a line formed by concentrated solute appears after the drying period. This phenomenon was first demonstrated by Robert D. Deegan and termed as the "**coffee ring effect**"(*63*). Fig 1.6 presents the typical coffee ring effect image. This mechanism of micro and nano particles within evaporating liquid droplets has many important applications.

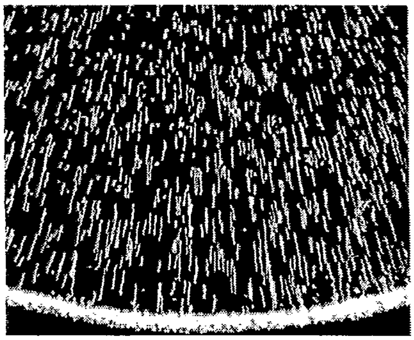

Figure 1.6 Spheres in water during evaporation (*63*)

By introducing the coffee ring mechanism, Park *et al.* (*64*) enhanced their production quality in synthesizing reproducible transistors with patterned active layers and source/drain electrodes. Also, Huang *et al.* (*65*) proposed a strategy for simply assembling single colloidal particle lines. This strategy can be applied in preparing large scale nano electronic devices such as vertical field effect transistors with individually addressable nanowire components. In their research, nano particles (silver particles in their experiments) were dispersed in organic solvent to produce a colloidal solution. Then, an appropriate amount of the colloidal solution was spread onto water surface. When the solvent had completely evaporated, a monolayer of nano particles was obtained on the water surface. After that, a substrate was dipped into this monolayer, and then raised by inducing the coffee ring effect; the nano particles would be concentrated in a pinned contact line. Through repeating these procedures for the whole substrate, uniform 1D arrays of particles with varieties of sizes from micrometers to nanometers were obtained.

The first model of the coffee ring effect was presented by Deegen *et al.* (*66*). In their experimental data, they suggested that only the ring size but not the shape would change according to the drop's volume. Therefore, with a known volume of liquid drop and liquid evaporation rate, the size of the ring composed by residues can be calculated. Recently, based on this approach, Popov (*67*) developed a more complete model for depositing patterns in evaporating drops of colloidal solution on a plane substrate. According to this model, the morphological characteristics of the deposition patterns are suggested as functions of the initial concentration of the solute, the initial shape of the drop, and the drying time period. The model was solved analytically for small initial concentrations of the solute and numerically for arbitrary initial concentrations of the solute. Also, in the latest research, Shen *et al.* presented that there is a minimum size of liquid drop required for coffee ring structure formation (*68*). If the drop size is too small, the evaporation rate of the liquid is much faster than the solute movement. All liquid would completely evaporate before the occurrence of outward replenished flow. Thus the coffee ring effect would cease to exist in small liquid drops.

1.5 Objectives of this work

With many applications of paper based analytical devices, there is still not sufficient fundamental research on particle transportation through paper media and factors that influence the transportation phenomenon such as paper properties, particle properties (i.e. surface charge, ionic strength etc) and environmental conditions (i.e. relative humidity, temperature). Therefore, this research focuses on understanding how and why the properties of paper and samples affect sample transport by using the existed theories such as Lucas Washburn's equation and DLVO theory.

Furthermore, as suggested by Fries (*29*), when solutions (or colloids) are transported in paper, the subsequent solution would keep being transported to the elution end (the position the capillary flow stops flowing forward) by a mass flow after the capillary flow stops. This mass flow took place in order to replenish the evaporation loss of liquid in early transported solution. The transport of subsequent solution would continue until papers were taken out from solutions. When latexes are eluted in paper, this mass flow does not only transport liquid but also carry suspended particles toward the elution end and further causes particle concentration. This research worked on understanding the influence of evaporation on latex transportation and deposition in paper porous media. Furthermore, model simulations are also conducted based on the model setup by Fries *et al.* (*29*) to investigate the maximum elution distances of latexes in paper when elution occurring at varying relative humidities. The influence of paper properties on latex maximum elution distance is also analyzed by this model.

Chapter Two: Methods

2.1 Instruments

2.1.1 UV-Vis

Beckman Coulter DU 800 UV/Vis Spectrophotometer was applied in all of our UV-Vis spectrum data analysis. All paper strip samples were analyzed by UV-Vis in order to monitor the distribution of particles deposition in paper after eluted in different conditions. First, controlled amounts of polystyrene (PS) particles were dissolved in Tetrahydrofuran (THF). Then the absorbance signals at 260 nm wavelength (absorption peak of benzene ring (*69*)) were plotted as a function of PS-THF solution concentration. Thus, calibration lines for four latexes were obtained for measuring the PS concentration was obtained. In order to investigate the dissolving efficiency of THF for deposited PS in paper, 0.1 mL of 80 (+) latex solution was dipped on a 1 cm^2 Whatman No 1 paper chip. The sample paper chip was dried in air and then was soaked in 2 mL THF solution for 24 hours to make sure all the PS particles dissolved. The absorbance spectra of PS-THF solution were measured at 260 nm. The obtained signal was then converted to concentration by the calibration line. The concentration obtained was well agreed with the 0.1 mL 80 (+) latex solution dipped on paper.

For paper samples analysis, the bottoms of paper strips (1 cm) where dipped in latex solution were cut off. Then, paper strip samples were separated vertically into 1 cm small chips and soaked in 2 mL THF for 24 hr in order to dissolve the deposited PS particles in paper. The absorbance of these PS-THF solutions at 260 nm was measured by spectrophotometer and converted to concentration by calibration lines. Therefore, the concentration of each chip can be obtained. Fig 2.1 shows UV-Vis spectra of 80 (+) latex (the synthesis procedures and properties of latexes are introduced in Chapter 2.3) with concentration 0.45-7.29 ($\times 10^{12}$ amount/mL) and the calibration cur)ve of 80 (+) with standard deviation (R^2).

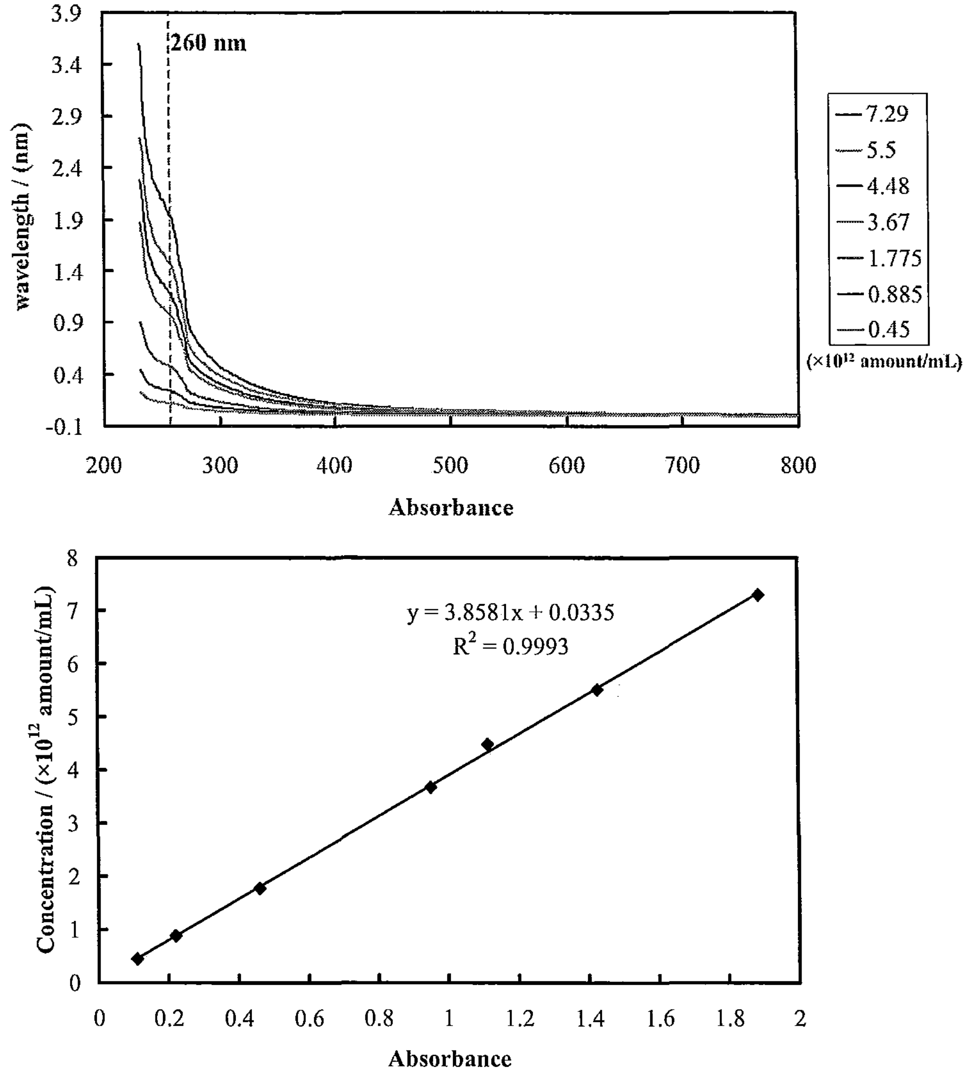

Figure 2.1 (a) UV-Vis spectra of 80 (+) latexes with concentration 0.45-7.29($\times 10^{12}$ amount/mL) (b) Calibration curve of UV-Vis absorbance as a function of 80 (+) latex concentration

2.1.2 Dynamic Light Scattering (DLS)

Brookhaven Dynamic Light Scattering which has BI-9000AT auto-correlator and 35 mw laser was applied to analyze the particle size of latexes. Data was collected and analyzed by BIC dynamic light scattering software 9kdlsw32 (version 3.34). A built-in cumulative statistical method was applied to analyze data. All measurements were performed under 25 ℃, maintained by NESLAB water bath.

2.1.3 Electrophoretic Mobility

The electrophoretic mobility of latex solutions was measured by applying the Brookhaven ZetaPALS (USA) instrument in PALS (phase analysis light scattering) mode (PALS software version 2.5). The reported mobility was the average of 10 cycles; each cycle was conducted with 20 scans. Each latex was measured in order to obtain the mobility data for further data analysis. The experiments for analyzing the mobility of synthesized polystyrene latexes were performed in pH = 7.5 which was maintained by 0.1mM KH_2PO_4 and NaOH buffer. The preparation of buffer is introduced in Chapter 2.3.1

2.1.4 SEM

Jeol 7000F FE-SEM at the Brockhouse Institute of Materials Research was applied in obtaining all SEM images. Two 3 x 3 mm^2 pieces of paper were cut from the top and middle (depend on eluted distance) of elution path in paper strips. The two pieces of paper were mounted on SEM sample stage by carbon tape. 4 nm of platinum particles layer was coated on the surface of whole stage for enhancing the conductivity. Next, the stage was put into the SEM chamber for monitoring the morphology of particle deposition in paper under different elution situations.

2.1.5 Confocal Microscopy

The samples for obtaining cross section images by confocal were prepared by Ms. Marcia West. First, two small pieces in the size of 2x10mm^2 were cut form paper strips which had eluted 80(+) and 135 (-) latexes in atmosphere with humidity around 45%. Small pieces of paper are cut at the middle of the elution path on each paper strips (i.e. if elution distance is 50 mm, the cutting region would be approximately from 24.5 mm to 26.5 mm). Next, the small pieces of paper were put in a flat embedding mold. To fix the sample, the mold was then filled with Spurr's Epoxy Resin and allowed to polymerize over night in a 60℃ oven. The embedded samples were placed into the chuck of an ultramicrotome and excess resin trimmed away with a glass knife to expose the cross-section of the paper.

Confocal imaging was performed using an inverted single photon fluorescence microscope (DMI 6000 B, Leica, Wetzlar, Germany) with a 20X objective. The fluorescence of PS particles was excited by built-in Argon Laser at 488 nm and the emission band was set at green range, which was done through a prism-based spectrometer that allowed continuous tuning from the near UV to the near IR. To prepare for imaging, the coverslip was placed in a bracket and the paper sample was fixed on top of it.

2.2 Materials

2.2.1 Whatman No. 1 filter paper

Whatman No. 1 filter papers (46 x 57 cm^2, Cat. No. 1001917) were used as the paper sample in all elution experiments. These filter papers are manufactured from high quality cotton linters which have been treated to achieve a minimum alpha cellulose content of 98%. The properties of Whatman No. 1 are listed as follow:

Width (W): 0.02 m
Average thickness (δ): 1.8 $\times 10^{-4}$ m
Porosity (ϕ): 0.7422 (Porotech Ltd.)
Average capillary radius (Rs): 7.609×10^{-6} m (Porotech Ltd.)
Permeability (K): 0.131 $\times10^{-12}$ m^2
Contact angle (θs): 0° (Liukkonen, 1997)

The porosity and average pore radius of Whatman No. 1 were obtained from

Porotech Ltd. Fig 2.2.1 shows the differential pore volume distribution as a function of pore radius of Whatman No. 1 filter paper which also obtained by Porotech Ltd.. The blue line is the experimental data obtained from paper saturated by deionized water. The pore volume distribution shows that pore size in wet paper are narrowly distributed in 3.2 to 7.9 μm. The permeability of Whatman No. 1 was obtained by measure the h (elution distance) and t (time) relationship when deionized water capillary rose in Whatman No. 1 paper strips. The H and t data was then substitute in the equation suggested by Fries *et al.* (*29*):

$$h^2 = \frac{4\sigma\cos\theta_s}{\phi\mu}\cdot\frac{K}{Rs}\cdot t \qquad \text{Eq 2.2.1}$$

The results of h and t relationship are shown in Fig 2.3. Based on these results and other known properties of Whatman No. 1, the permeability of Whatman No 1 is obtained as 0.131×10^{-12} m^2.

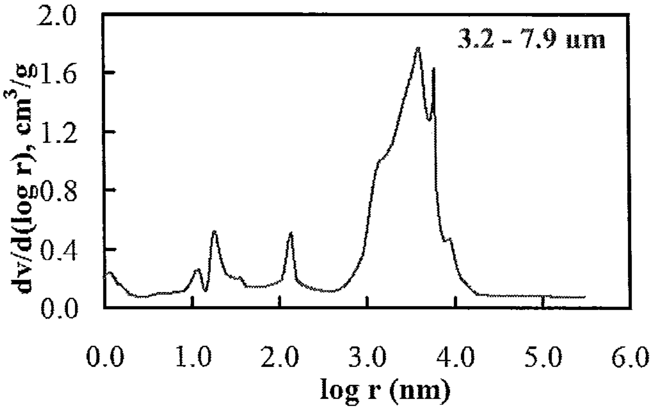

Figure 2.2 Pore size distribution of Whatman No 1 obtained from Porotech Ltd.

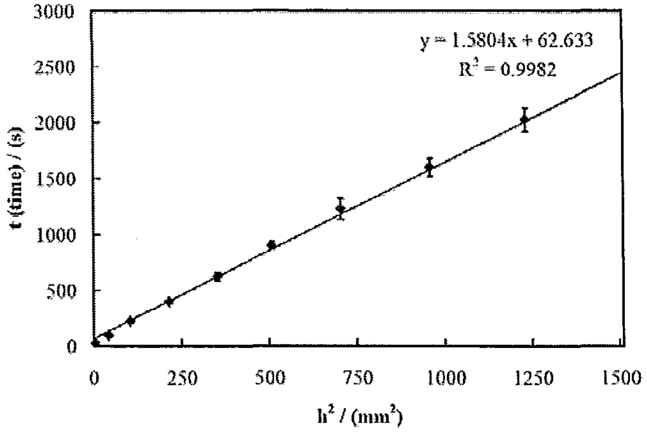

Figure 2.3 Deionized water elution distance in Whatman No. 1 paper strip as a function of elution time

2.2.2 Polystyrene

Four different Polystyrene (PS) latexes have been synthesized for analyzing the particle movements in porous paper media under various conditions. All recipes for synthesis of PS particles are shown in Table 2.1. The synthesis procedures are presented as following: Styrene (St) (99%, Sigma-Aldrich, S4972) was purified by vacuum distillation. 2, 2'-Azobis (2-methylpropionamidine) dihydrochloride (V50) (97%, Aldrich, 440914), (Vinylbenzyl)trimethylammonium chloride (VBTMAC) (99%, Aldrich, 458694), Sodium dodecyl sulfate (SDS) (99%, Aldrich, 436143), Potassium persulfate ($K_2S_2O_8$) (99%, Sigma-Aldrich, 216224) and Fluorescein dimethacrylate (FD) (95%, Aldrich, 570249) were all purchased from Sigma-Aldrich and used as received. Polymerization was conducted in a 250 mL three-necked flask equipped with a condenser, two rubber stoppers one for N_2 purge, the other for needles purging connected to the syringe pump), and a magnetic stirring bar. For cationic PS particle synthesis, first St, water, VBTMAC, V50 and FD were added at 70°C. After 30 minutes (80 nm) and 45 minutes (120 nm) of polymerization, the additional composition, St equipped in a 20mL syringe, was added by the syringe pump in 6 hours, and then let the reactions last for 17 hours. The final reaction mixture was dialyzed for at least one week, until the supernatant conductivity was no more than 5 μS/cm. For anionic PS particle synthesis, St, water, SDS, Fluorescein dimethacrylate and $K_2S_2O_8$ were add at 70 °C for 24 hours for polymerization. The final products were purified by ultracentrifugation. The particle size, mobility and Electrophoretic mobility (EM) values were monitored by DLS and ZetaPlus analyzer.

Table 2. 1 Recipes for PS particles synthesis

	water (g)	St (g)	FD (g)	VBTMAC (g)	$K_2S_2O_8$ (g)	SDS (g)	additional St (g)
80(+)	83	0.5	0.0229	0.3	N/A	N/A	11
120(+)	83	0.5	0.0229	0.3	N/A	N/A	11
60(-)	100	3.6	0.01	N/A	0.105	0.12	N/A
135(-)	100	3.6	0.01	N/A	0.105	0.3	N/A

Table 2.2 shows all properties of synthesized PS latexes. Concentrations of latexes were analyzed by measure the weight of completely dried particles in each latex solution. First, the weights of each 10 mL latex solution were placed in 80℃ oven for 20 min to evaporate all water content in latex solution. Next, the weights of those completely dried latex particles (W_{LP}) were measured and divided by particle volumes which were calculated by sphere volume formula ($4/3\pi R^3$, where R is the radius of particles). Finally, the amount of particles in 10 mL latex solution was obtained. It has to be noted that the concentrations of 80 (+) and 135 (-) are similar and surface charge of those latexes are opposite. Thus, those two latexes are chosen to apply in experiments which are set up for understanding the influences cause by salt contents of paper and flow velocities of elution flow.

Table 2. 2 Properties of PS particles

	Particle diameter (nm)	polydispersity	concentration (number/mL)	electrophoretic mobility ($10^{-8}m^2s^{-1}v^{-1}$)	Std error
80(+)	76.9	0.126	2.9×10^{14}	2.17	0.07
120(+)	120.8	0.103	8.5×10^{13}	2.04	0.12
60(-)	53.8	0.13	1.5×10^{15}	-3.5	0.05
135(-)	133.3	0.106	2.1×10^{14}	-4.83	0.14

2.2.3 Buffer

All synthesized PS latexes were storied in 0.1mM KH_2PO_4/NaOH buffer solution (pH=7.5) for further analysis (i.e. particle diameter and mobility). The preparation of the buffer was described as follow: First, 0.4 g NaOH was dissolved in 100 mL deionized water to produce 0.1 M NaOH solution. Next, 40.9 mL of this solution was mixed with 50 mL 0.1 M KH_2PO_4 solution and then diluted to 100 mL to produce buffer. The pH of this buffer was monitored by pH meter and adjusted to 7.5 by adding 0.1 M NaOH and 0.1 M KH_2PO_4 solutions. Then 1 mL buffer solution was diluted with 100 mL deionized water to become 0.1 mM. The pH of the produced buffer was checked again after conditioning at room temperature for 24 hours to make sure there was no further change.

2.3 Elution

Whatman No 1 rectangle filter paper (46 x 57 cm^2, Cat No 1001917) was cut into 140 mm x 20 mm paper strips with approximately 180 μm of thickness and 0.22 gram of weight. The paper strips were cut by following the machine direction of the Whatman no 1 filter paper. Back (*2*) observed that flow velocity of papers in their research is 5-20 % higher in the machine direction than in the cross-direction. Thus, there would be more particles transported in capillary flow of latex solution in machine direction than in cross-direction. Therefore, the influence of particles movement may easily be observed. Next, those paper strips were set up (hanging) on the rack for vertical elution (see Figure 2.3 (a)). In elution, 1cm of paper strips were dipped into latex solutions with pH = 7.5, which then induced the latex solution flowing up by the capillary force. Also, the experiments of time versus eluted distance were conducted by eluting latex solutions in paper. The paper sample above air-latex solution interface was marked per 5 mm (Fig 2.2.1 (b)). Once the flow reached the marks, the corresponding time were recorded immediately. Each elution experiment was repeated four times to get the averages as well as error bars for final results.

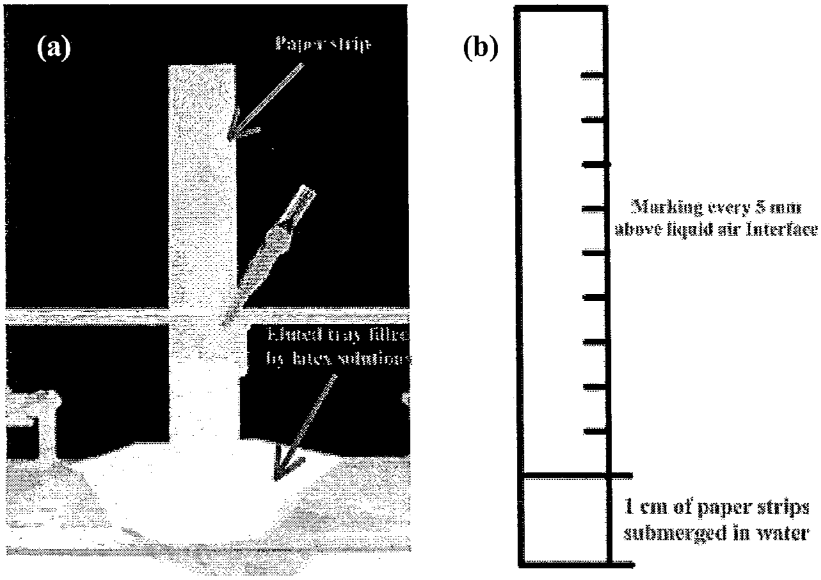

Figure 2.4 (a) elution device (b) sketch of strips in measuring time in controlled elution distances experiments

2.3.1 Particle properties

ZetaPlus analyzer was applied to analyze the electrophoretic mobility values of four latexes. Then Whatman No. 1 paper strips were dipped into those latex solutions for 1 hour elution. Next, UV-Vis was applied for analyzing the particle deposition on those paper strips.

2.3.2 Flow velocity

Paper strips with 5 mm and 10mm widths (25 mm length) narrow rectangular shapes in the middle were cut form Whatman no 1 filter paper strips with similar length and thickness as strips applied in other experiments (Fig 2.4). These were prepared to investigate the influence of particles deposition caused by the flow velocity. The flow velocities of each paper strips were obtained by recording the time when deionized water elution flow passed the 5 mm interval marks in each paper strips. Then, 80 (+) and 135 (-) latexes were eluted in those strips and by following the UV-Vis procedures, particles deposition in 10 mm vertical divided paper strips (elution path) were analyzed.

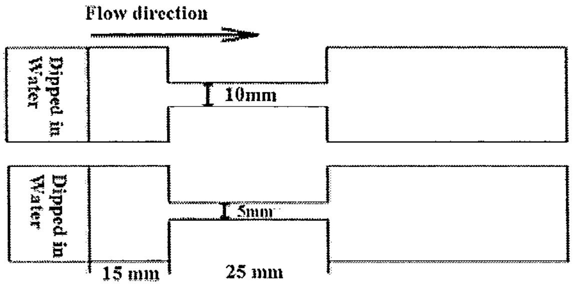

Figure 2.5 Paper strips with 5 mm, 10mm narrow rectangular

2.3.3 Ionic strength

For understanding the ionic strength affecting particle movement during elution in paper porous media, the quantitative KCl was induced on paper strips before elution by following procedures. Five different (2M, 1M, 0.5M, 0.2M and 0.1M) concentrations of KCl solutions were firstly prepared. Paper strips were separately pre-soaked into these five solutions and deionized water, and then dried in the oven at 60 ℃ for 15 min. Then, those completely dried paper strips were dipped into 80 (+) and 135 (-) latexes for 1 hour of elution. Because the maximum water imbibitions of paper strip are constant, once the concentrations of pre-soaked KCl solution are different, the KCl contents in dried paper are also different. Furthermore, during elution, KCl induced in paper would be dissolved when latex solution flowed through and lead to alterations of ionic strength during latex elution. Therefore, with different KCl contents in paper strips, the influence of ionic strength on particle movement during elution was able to observe. In each trial, time was recorded at the point where the latex solution reached the marks with 5 mm interval. Besides, the final elution distance of each trial was also recorded. After elution, the paper strip samples were first observed under SEM and confocal microscope. Then, the UV-Vis was applied to analyze particle deposition in each position of paper from different trials.

2.3.4 Humidity influence

In order to understand mechanisms that lead to concentrated particles in the elution end, the experiments of allura red solution eluted in limited evaporation rates have been done. Solution of allura red is made by dissolving 0.15 g of Allura Red anionic dye (80%, Sigma-Aldrich, 458848) in 60 ml deionized water with 0.1mM, pH = 7.5 KH_2PO_4/NaOH buffer. In these experiments, allura red solution was eluted by paper strips sealed by plastic bags (evaporation is limited), and other paper strips without coverage as a control group. This elution took place for 1 hour with around 45% (monitored by DRETAC hygrometer) relatively humidity at 25℃.

In order to understand how evaporation leads to the concentration of dyes and particles on the eluted end. The experiments of dyes eluted in wet paper strips had been conducted. Sketch of this experiment is shown in Fig 2.5. In these experiments, a series of black horizontal lines spaced out with 20 mm intervals were drawn across a long vertical strip of paper with water insoluble ink (Fig 2.5 (a)). The first vertical black line followed by the series of black lines is either drawn 20 mm from the centre of the paper strip (strips (I) and (II)), or drawn 40 mm from one end of the paper strip (strips (III) and (IV)). Next, paper strips were submerged in deionized water to make the paper saturated by water. Then, dye solutions (Allure Red (anionic), concentration= 2.5 g/L pH= 7.5 or Methylene blue (cationic) concentration= 2.5 g/L pH = 7.5, prepared by Methylene blue dye (Sigma-Aldrich, M9140)) was placed on the based black line on each saturated paper strip. Finally, the center of strip (I) was dipped into deionized water and the rest parts of paper strips were horizontally fixed above water for 30 min (Fig 2.5 (b)) with 45% (monitored by DRETEC hygrometer) relatively humidity at 25℃. Also, the bottom 10 mm of strip (III) was dipped into deionized water vertically for 30 min in the same environments.

Furthermore, latex elution was conducted in ESEPC platinous sterling series temperature and humidity chamber (ESEPC chamber in short) where the relative humidity and temperature were well controlled during elution period. The purpose of these experiments is to understand the influences of particles concentration in the elution end caused by varying humidity. At the beginning, the relative humidity in ESEPC chamber was set at 35%, 50%, 75% and 100% (machine limit), respectively, at 25℃, and run for 20 minutes for stabilization. In the mean time, four latex solutions (80(+), 120(+), 70(-), 135(-)) were filled in the trays. After confirming the stabilization of humidity in ESEPC chamber, paper strips were dipped into latexes solution and then the trays were moved to chamber immediately so as to minimize the errors affected by the environmental humidity outside of the chamber. The paper strip samples were collected after 1 hour and 2 hours of elution period. The elution distances of particles were then recorded. Finally, followed by the UV-Vis sample preparation and analyzing procedures introduced above. UV-Vis was applied for analyzing particles deposition at elution end in paper from different trials. Also, in order to propose a strategy to reduce samples lose while transporting in paper channel, as well as increase sample concentration for enhancing the detected intensity in array area. The 80 (+) latexes were eluted in paper strips with evaporation limited device for 1 hr and those strips were analyzed by UV-Vis.

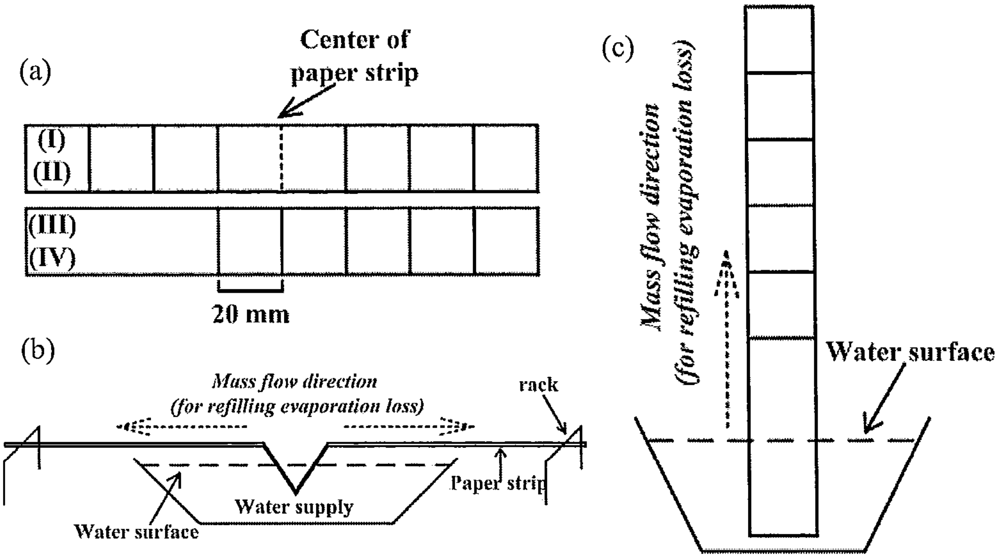

Figure 2.6 sketch of dyes eluted in wet paper strips (a) paper with based black line, (b) device of horizontal elution, (c) device of vertical elution.

Chapter 3 Particle elution in paper

3.1 Particle surface potentials and flow velocity

Abstract

In this chapter, the influence of latex surface potentials and flow velocity on deposition and transportation during latex elution in paper is discussed. Particles surface potentials are reflected by their mobilities. Our experimental results showed that higher deposition was observed when particles with higher positive mobilities were eluted and vice versa. The influence of flow velocities on particle deposition during elution was also studied. The flow velocity was controlled by varying the shapes of paper strips. The experimental data shows that flow velocities had no obvious influence on latex deposition and transportation.

3.1.1 Particle properties

Results

In order to understand the influences of latex surface potentials on particle transportation during elution in paper porous media. Latexes with different surface potentials were eluted on Whatman No. 1 paper strips for 30, 60, and 120 minutes (where cationic particles were indicated with (+) and anionic particles were indicated with (-) and the particles surface potentials are reflected by their mobilities). The details of those latexes as well as the experimental setups were presented in Chapter 2.2 and 2.3. Table 3.1 shows the elution distances of water (D_w) and latexes (D_p). After 30 minutes of elution, D_w became almost constant at 50 mm which suggested that water did not travel any further after 30 minutes. Table 3.1 also shows that D_p of 80(+) is larger than 120(+) during the same elution period. However, there was no significant difference on the D_p values of anionic particles.

Table 3.1 Travel distance of water (D_w) and latex (D_p) during 30, 60 and 120 minutes elution

	80 (+)	120 (+)	60 (-)	135 (-)
30 min D_p (mm)	43	24	50	50
30 min D_w (mm)	50	50	50	50
60 min D_p (mm)	48	36	50	51
60 min D_w (mm)	49	48	50	51
120 min D_p (mm)	48	36	50	51
120 min D_w (mm)	49	46	50	51

Fig 3.1 shows the particle deposition of different latexes in the elution path. As shown in Fig 3.1, the rank of particle depositions from high to low in 0 – 40 mm of the elution path is 120(+) > 80(+) > 60(-) ≒ 135(-).

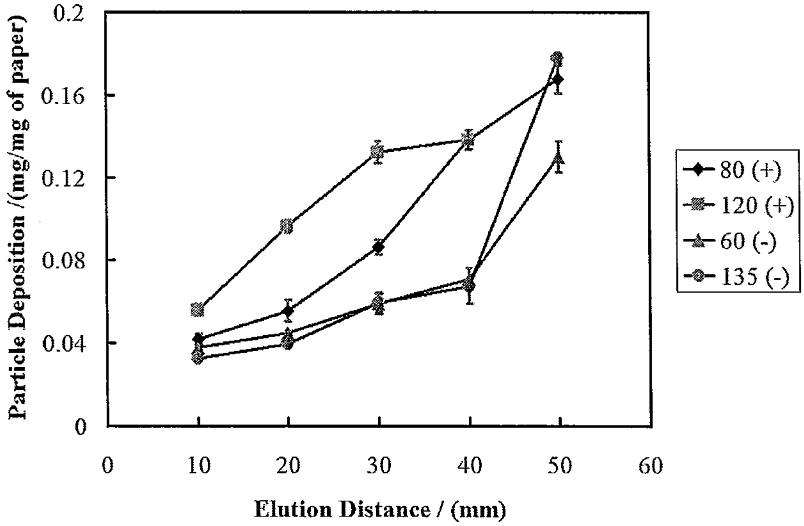

Figure 3.1 Particle deposition along the 10 mm divided paper strips after 1 hour elution of latexes (80 (+), 120 (+), 60 (-) and 135 (-))

Discussion

Before understanding the influence of other factors on particle transportation in paper strips, the influences caused by the properties of latex particles have to be clarified. Herzig *et al.* suggested that particle deposition during transportation in porous media is controlled by the **SR value** (*35*), which is the ratio of the pore size (the average pore size of Whatman No 1 is 7.609 um) over the particle size. Details of this theory are presented in Chapter 1. In our experiments, SR values of four different latex particles are in the same range of 0.01-0.04, which means that particle deposition is dominated by Brownian movement. Therefore, the effect of particle sizes can be neglected in our experiments.

Furthermore, water elution distances (D_w) were almost the same in four different latex elutions, which suggests the capillary forces acting on each trial were approximately constant. However, there are some differences that were observed in particle travel distances (Dp) between particles. Hence, there must be some other factors other than capillary forces affecting the particle movement.

The deposition of anionic particles on paper fibers are repulsed by anionic paper surfaces. On the contrary, anionic paper surface attracts cationic particles which induced particle depositions. Alince *et al. (62)* described that particle deposition caused the "sizing effect" that retards water penetration in paper. This retardation would be amplified with increasing amounts of latex deposition. This phenomenon was also observed in our experiments that higher particle depositions were obtained in paper strips which eluted particles with higher positive mobility. This further led to a decrease in elution distances in those paper strips (Table 3.1). When anionic particles were eluted in paper, anionic paper fiber surfaces repulsed anionic particles from depositing. Thus, both particles were able to reach the eluted end which is the longest distance elution flow can travel.

In a study on the transportation of bio colloids through porous media, Sharma *et al.* (*54*) found a high correlation between surface charge density and transportability. In the research conducted by Huysman *et al.* (*71*), deposition of anionic bio colloids on cationic porous media (clay) rose with the increase of their anionic charges. This increase of colloid deposition was attributed to the enhanced electrostatic attraction between anionic colloids and cationic groups of porous media (clay). Similar phenomenon can also be found in our experiments. As shown in Fig 3.1, the amount of latex deposition ranked from high to low as 120(+)>80 (+)>60 (-)≒135 (-) which is simulated as the rank of particle mobility.

3.1.2 Flow velocity

The research done by Bhagat (*55*) showed that in micro channel filtration systems, lower flow velocity would lead to more particle deposition. Muller (*56*) reported that the capillary flow velocity can be controlled by the shape of paper strips. He suggested that restricting the width of paper channels would cause acceleration in flow velocity. Therefore, latexes had been eluted in paper strips with different widths in order to study the effects of flow velocity on particles deposition. Different shapes of paper strips were made to control the flow velocity during particle movement in the elution process. The experimental details are shown in Chapter 2.3.2.

At first, deionized water was eluted in paper strips with 5 mm and 10 mm narrow widths in the middle. The eluted distances as a function of time were shown in Figure 3.2. Since the curves in Fig 3.1.2 represent the relationship between distance and time, slopes of those curves are the flow velocities during deionized water elution. By comparing with the flow rates in normal paper strips, it can be observed that the flow rate increased when water flowed through the narrow area (distance between 20-40 mm). This confirms Muller's research (*56*) showing that narrower paper strips result in higher flow velocity. Thus, 80 (+) and 135 (-) latexes were eluted on those differently shape paper strips to study the influences of flow velocity on latex movement. The black-white inverse florescence images of these experiments are shown in Fig 3.3(a). Figure 3.3 (b) and (c) show the particle deposition on 10 mm vertically-divided paper strips after eluting 80 (+) and 135 (-) latexes for 1 hour, respectively. It shows that the elution distances of 80 (+) would be reduced when elution took place in paper strips with narrowed widths in the middle (elution distance: 40 mm (strip with 5 mm width middle) and 42 mm (strip with 10 mm width middle) compared to 48 mm in 20 mm width paper strip). Furthermore, the particle depositions in narrow strips (ink and green dots) were higher than that of normal strips (blue dots). However, in 135 (-) elution results, the shapes of paper strips (flow velocity) did not affect either particle deposition or elution distance.

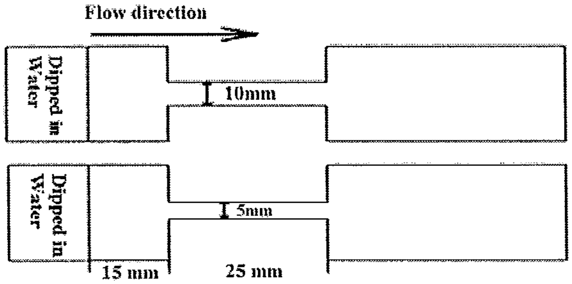

Recall Fig 2.4 Paper strips with 5 and 10mm narrow rectangular shapes

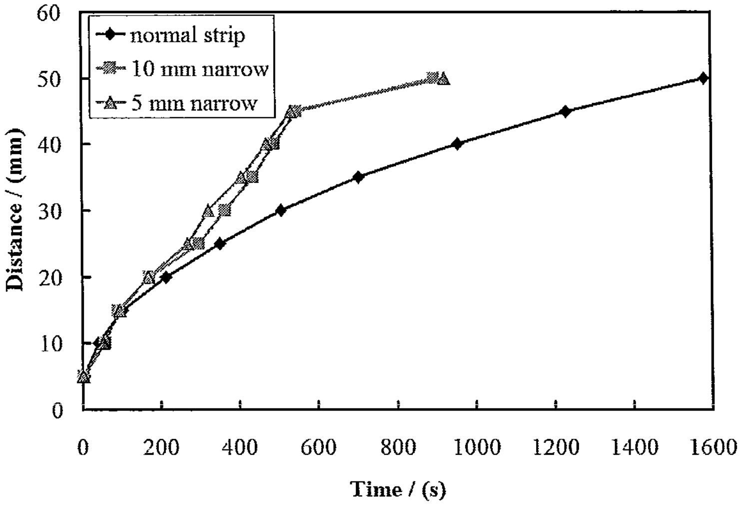

Figure 3.2 The elution distance as a function of time in water transport through paper strips with different shapes (5 mm, 10 mm and no narrow rectangular in the middle)

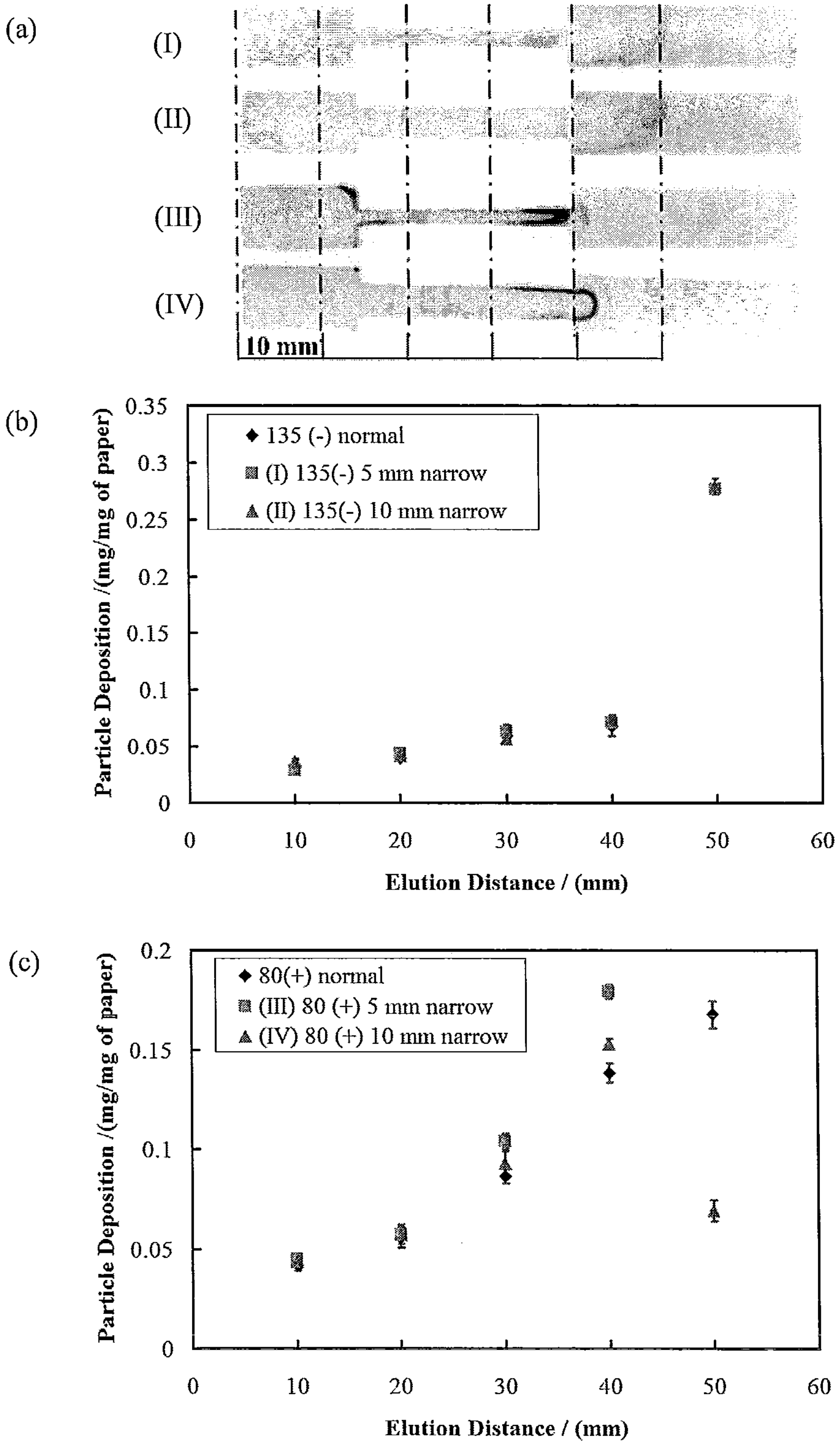

Figure 3.3 (a) The black-white inverse florescence images and (b) 135(-) and (c) 80 (+) particle deposition as a function of elution distance after 1 hour elution in paper strips with different shapes

Discussion

Figure 3.2 shows the capillary flow velocity of liquid would increase when eluted in paper strips with narrow middle. These results confirm Muller's results (*56*) that restricting the paper channel width would accelerate the flow velocity. Also, the research done by Bhagat (*55*) showed that in micro channel filtration systems, lower flow velocity would lead to more particle deposition. However, the experimental results shown in Fig 3.3 (b), there was no significant change of 135 (-) depositions after elution in differently shaped paper strips (different velocities). In Bhagat's experiment, the flow velocity of latexes was controlled form 0.1 to 10 mm/s to investigate the effects of flow velocity on filtration efficiency. However, in this study, the variation of flow velocity caused by different paper widths was in the range of 0.25 – 0.45 mm/s (Fig 3.2). Therefore, the changes in flow velocity led by different widths of paper might be too small to alter the amounts of anionic particle deposition.

In addition, the experiments of 80 (+) elution with different flow velocity show contradict results with Bhagat's research (*55*). Higher flow velocity in narrower strips suggests more particles would be transported upward during the same elution period which further increases particle deposition. This can be observed in our experiments that particle depositions of 80 (+) is higher in strips with the 5 mm and 10 mm narrow middle than that observed in normal strips (Fig 4.3 (c)). Also, the increase of particle deposition amplified retardation of elution flow penetration, thus the elution distance of 80 (+) was reduced when particles were eluted in the strips with 5 mm and 10 mm narrow middle. Consequently, we conclude that the increase in flow velocity by narrowing paper shapes would not decrease the quantity of anionic particle deposition. On the contrary, the narrower channel leaded to more deposition of cationic particles.

3.2 Ionic Strength

Abstract

According to the DLVO theory, varying the double layer thickness of particles would affect the energy barrier between particles and paper surfaces. This further influences the depositions of charged particles on paper porous media. In this chapter, the experimental data revealed that the particle (cationic and anionic) depositions increased when latexes flowed through paper strips with salt content (the salt dissolved when the latexes flowed through and thus increased the ionic strength of the elution flow). As the salt content increases, the particle depositions would be enhanced and the elution distances would reduce

Result

On a macroscopic scale, a theoretical assumption of capillary rise in porous media was developed in the last decade. In this research area, Lucas-Washburn's equation has been broadly applied to the analysis of liquid capillary flow through porous media (*20*). This equation shows that the fluid transported distance H(t) is proportional to the square root of the capillary time ($t^{1/2}$) ,

$$H(t) = \left(\frac{\gamma_{LV} R \cos\theta}{2\eta}\right)^{1/2} \sqrt{t} \qquad \text{Eq (3.2.1)}$$

Where γ_{LV} is the surface tension of the liquid, η is the shear viscosity, R is the pore radius, and θ is the contact angle between the liquid and the capillary media.

Figure 3.4 shows the H (water elution distances) and $t^{1/2}$ ($Time^{1/2}$) relationship of particles (80(+) and 135(-)) when eluted in paper strips, which were pre-soaked in different concentrations (0-2M) of KCl solutions. Since there is no significant difference between the results of elution in paper pre-soaked in 0M (no KCl) and less than 0.5M KCl, those results are not shown in Figure 3.4.

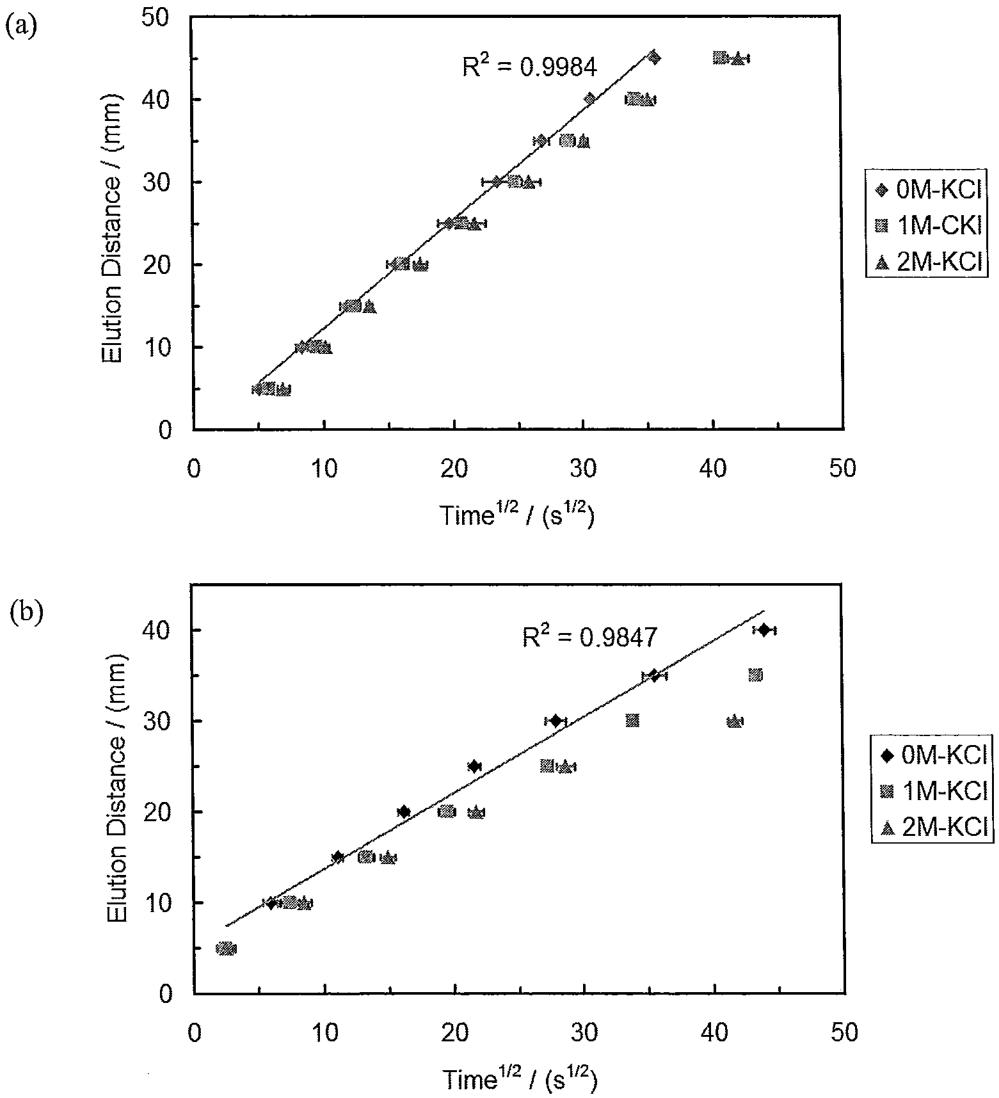

Figure 3.4 Elution distances as a function of $t^{1/2}$ for particles: (a) 135 (-) and, (b) 80 (+) in paper pre-soaked in 0M, 1M and 2M KCl solutions

As shown in figure 3.4, we observe that H and $t^{1/2}$ shows approximately a linear relationship (R^2: 0.9984(135(-)) and 0.9847(80(+))) when the latexes were eluted in paper strips with no KCl. This suggested that the latex elution flow in the no-salt strip followed Lucas-Washburn's equation. However, the H and $t^{1/2}$ relationship changes from linear to nonlinear when the latexes were eluted in salt-containing paper strips; nevertheless, the higher the salt content is, the more the slope decreases.

Fig 3.5 (a) shows the particle depositions of 135 (-) as a function of elution distances in paper strips with different KCl contents. The data was collected every 10mm of the elution path. As shown in Fig 3.5 (a), with more KCl content on the paper strips, there would be more particles deposited during the 1 hour elution. Moreover, black-white inverse florescence images of 135 (-) (Fig 3.5 (b)) also show the particles elution distance decreases with the increasing in KCl contents on paper.

Fig 3.6 (a) shows particle depositions of 80 (+) after eluted in paper strips with different salt contents as a function of elution distance. The elution distance was divided into 10 mm spaces. In 0M-KCl (no salt) paper strips (blue dots); it shows particles concentrated on the top 20 mm of the paper strips (30-50 mm of the elution path) after 1 hour elution. Moreover, in the results of paper strips pre-soaked in 0.5M to 2M KCl solutions, the increase in particle depositions was clearly observed between 20-40 mm of the elution path. Black-white inverse fluorescent images of 80 (+) after eluted on paper with different salt content are shown in Fig 3.6 (b). Particles and water moving distances both decreased with the increase of KCl contents.

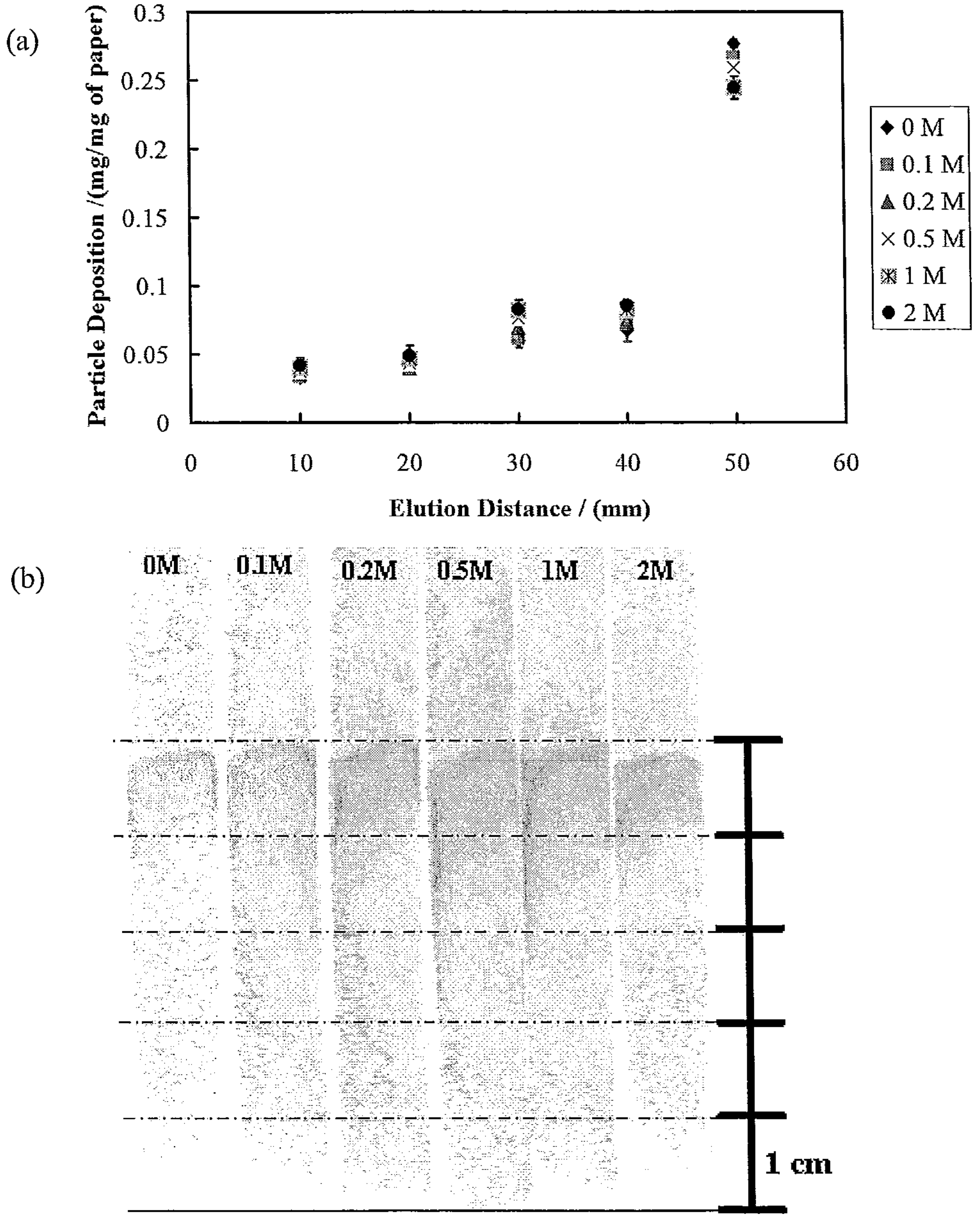

Figure 3.5 (a) particle deposition of 135 (-) latexes in vertically 10 mm divided paper strips after 1 hr elution (b) the black white inverse fluorescence image of 135 (-) eluted in 0M - 2M paper strips

(a)

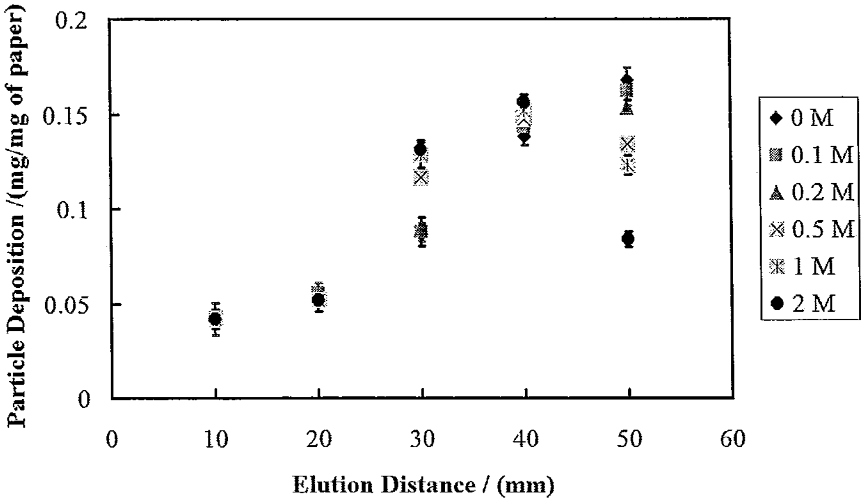

(b)

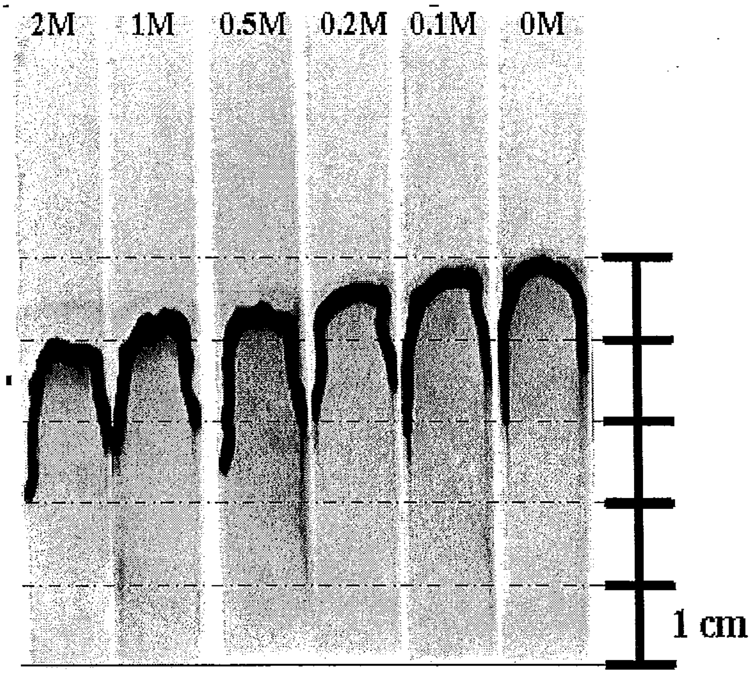

Figure 3.6 (a) particle deposition of 80 (+) latexes in vertically 10 mm divided paper strips after 1 hr elution (b) the black white inverse fluorescence image of 80 (+) eluted in 0M - 2M paper strips

Fig 3.7 (a) and (b) are SEM images of 135(-) particles after eluted in 0M-KCl and 2M-KCl paper strips, respectively. Particle aggregation is only observed in the 2M-KCl paper strip. The SEM images of 0M and 2M-KCl paper strips after eluting 80 (+) latexes are shown in Fig 3.8, respectively. In the image of 80(+), after eluted in the 0M-KCl paper strip (Fig 3.8 (a)), deposition of particles formed a monolayer structure on the paper fiber surface. However, when 80(+) particles were eluted in the 2M-KCl paper strip (Fig 3.8 (b)), the amounts of particle deposition increased significantly. Also, it was noted that some pores in paper media were even blocked by particles.

Furthermore, Fig 3.9 shows the fluorescence images obtained by confocal microscopy after the latexes were eluted in 0M-KCl and 2M-KCl paper strips. In fig 3.9 (a), it can be observed that in the 0M-KCl paper strip, 135(-) particles deposited only when trapped by paper fibers. Fig 3.9 (b) shows that particles deposition increased when particles were eluted in 2M-KCl paper strip. In images of 80(+) elutions, it can be seen that the deposition layer is thicker in the 2M-KCl paper strip than that in the 0M-KCl paper strip (Fig 3.9 (c) and (d)).

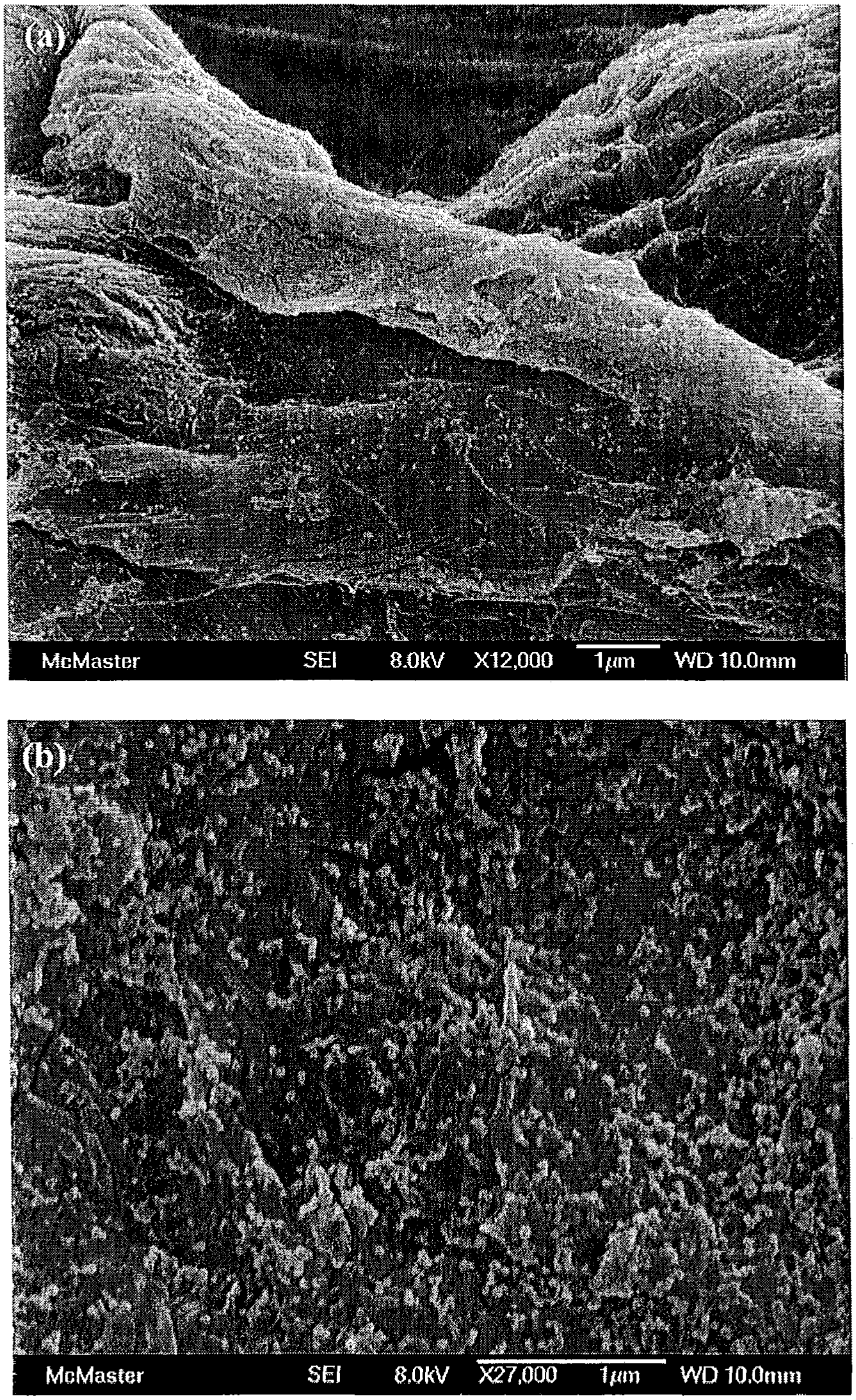

Figure 3.7 (a) 135(-) eluted in 0M-KCl paper strips for 2 hours, (b) 135 (-) eluted in 2M-KCl paper strips for 1 hour

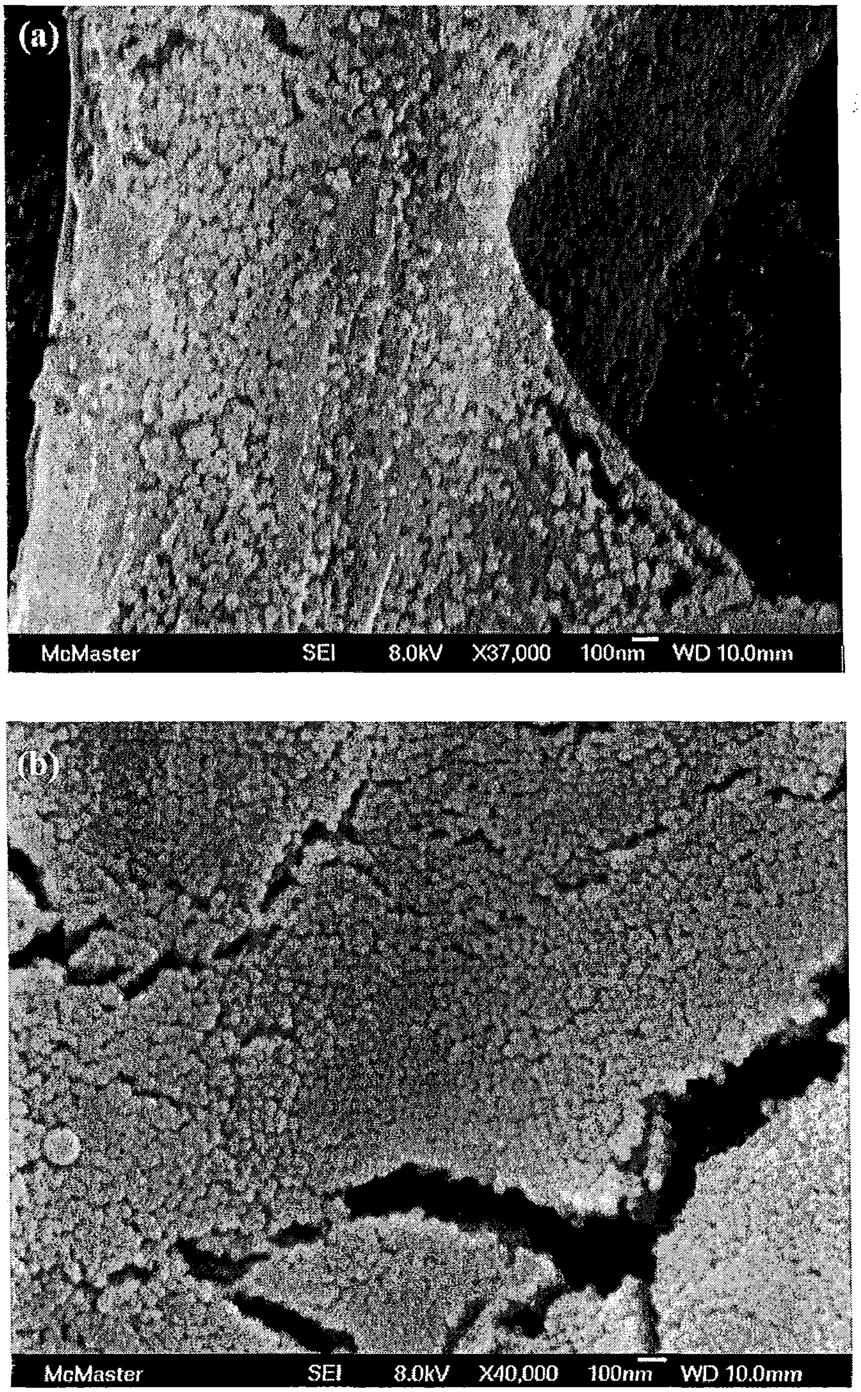

Figure 3.8 (a) 80(+) eluted in 0M-KCl paper strips for 2 hours, (b) 80 (+) eluted in 2M-KCl paper strips for 1 hour

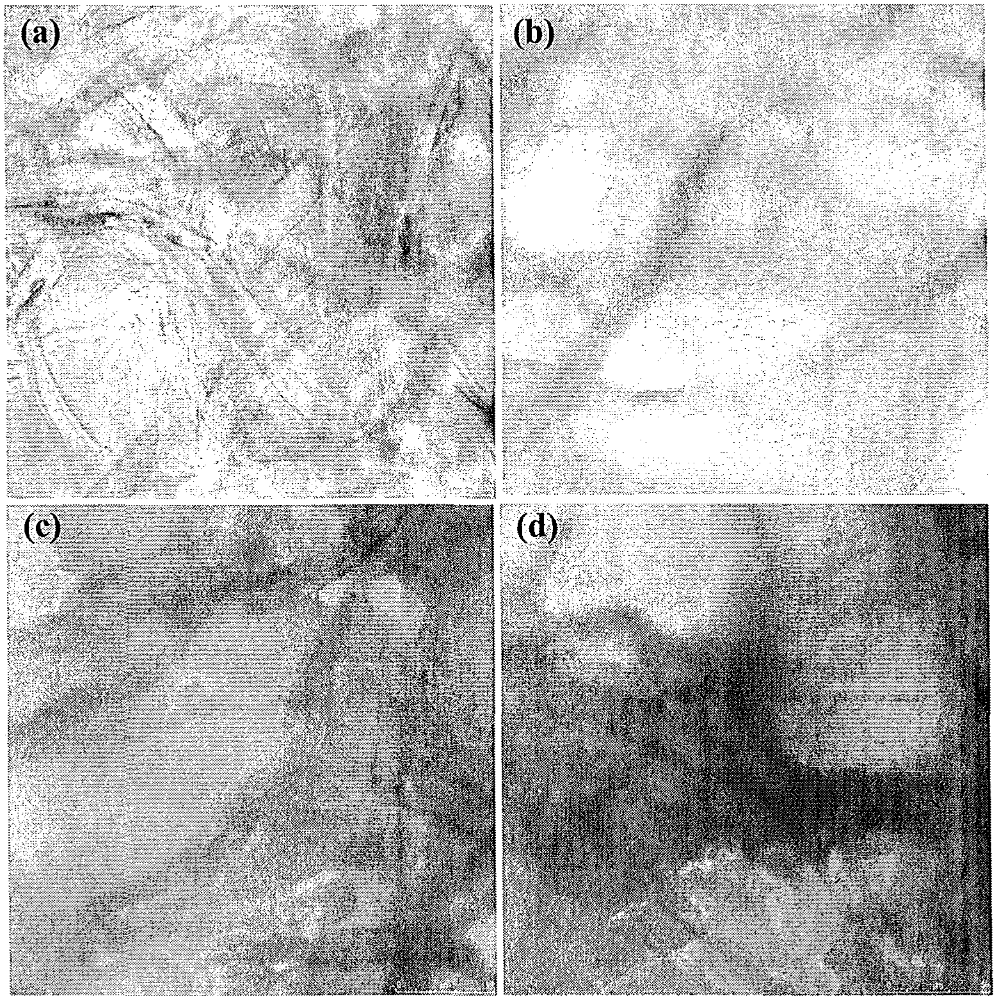

Figure 3.9 Fluorescence images of (a) 135(-) eluted in 0M-KCl paper, (b) 135(-) eluted in 2M-KCl paper, (c) 80(+) eluted in 0M-KCl paper, and (d) 80(+) eluted in 2M-KCl paper,

Discussion

In the last few decades, DLVO theory has been applied to explain comprehensive phenomenon of particle movement in porous media (*38*). Details of DLVO theory were already presented in Chapter 1. In short, the DLVO theory has been used to describe the net interactions between particles and the porous media surface (paper fiber with anionic surface charge in our research). The net interaction is the balance between two additive forces, F_{VAW} caused by van der Waals interactions (generally attractive) and the repulsive interactions "F_{DL}" from the overlap between the electrical double layer of particles and paper fibers (repulsive for anionic latex and attractive for cationic latexes). While latexes are transported through the paper network, a charged surface of particle is neutralized by the oppositely charged ions covered on the surface. Because of the thermal motion and electrical attraction of counter ions, an accumulated layer forms on the charged surface (*73*). This layer is called the Gouy–Chapman diffuse electric double layer. In our research, deposition of anionic particles on to the anionic paper surface then depends on the thickness of this double layer. Once anionic particles overcome the repulsive force and enter the electrical double layer, van der Waals forces between particles and surfaces would dominate particle movement, resulting in particle deposition on the paper surface. Many research suggested that the thickness of the electrical double layer would be reduced in high ionic strength situations (*33*) and the secondary minimum is forced closer to the media surface. Consequently, more anionic particles were able to move close enough to the media surfaces for the van der Waals attraction to overcome the repellence of electrical double layer and lead to more deposition

According to our experimental results, we suggested that during latex eluted through paper with KCl content, the coated KCl were dissolved once contacted with the elution flow and enhance the ionic strength of the elution flow. Therefore, the deposition amounts of anionic latexes would increase as well. As can be observed in Fig 3.5 (a), in the results of anionic particle elution in paper with KCl content, there were increases in the deposition amount observed. Furthermore, the increase in deposition would rise once the concentration of pre-soaked KCl solution was increased. The SEM and confocal microscopy images also show similar results that there were obviously more depositions of 135 (-) particles in 2M-KCl paper strips than that in 0M-KCl paper strips (Fig 3.7 and Fig 3.9 (a) and (b)). Besides, the congregation of 135 (-) particles in 2M-KCl paper strips can be observed in the SEM images (Fig 3.7 (b)). This phenomenon is because of the increase of ionic strength also reduces the particle-particle repulsive force. Moreover, the influence of salt content on the movement of latex elution flow in paper can also be observed. As shown in Lucas-Washburn's equation, for liquid transporting through a constant pore radius media, H and $t^{1/2}$ has a linear relationship. In Fig 3.2.1 (b), when 135(-) particles were eluted in the paper strip without KCl, the H and $t^{1/2}$ are approximately in a linear relationship which means there is only a little influence on latex eluted flow caused by particle deposition. As mentioned in Chapter 3.1, an increase of particle depositions would retard subsequent liquid penetration in paper. This was shown by the non-linear relationship of H and $t^{1/2}$ when 135 (-) was eluted in paper with KCl (Fig 3.2.1 (a)). This non-linear relationship was amplified by raising the pre-soaked KCl solution concentration (which increased the KCl contents in paper and led to the increase of particle deposition). This agreed with UV results presented before that the depositions of 135 (-) were enhanced when eluted in paper with more KCl content.

When 80(+) particles were eluted in paper, due to the anionic electrical charge from the paper surface, the electrical double layer force also acted attractively. Therefore, at the beginning of elution, once 80 (+) particles were eluted through paper, particles attracted by paper fibers and result in deposition. However, the deposited particles would influence the deposition of the latter following latexes particles flowing through. Once cationic particles deposit on paper fiber surfaces, due to the repulsive particle-particle interactions, the particle deposition layer would repulse other suspended particles from depositing. This surface exclusion phenomenon is termed blocking (*50, 51*). Blocking restricts particle deposition to a single monolayer structure and let suspended particles flow further. We can observe the monolayer structure caused by blocking in our SEM images (Fig 3.8 (a)). This monolayer structure of deposition was also observed by Alince *(60)*. He studied cationic colloidal particle deposition on pulp fibers and found that the amounts of cationic particle deposition on pulp fibers would reach a plateau. Particle deposition amounts in that plateau are close to the amounts of a monolayer of latex particles that fiber surfaces able to accommodate.

When cationic latex eluted in paper with KCl content, the dissolved KCl would increase the ionic strength in elution flow. Thus, the electrostatic interaction between particles and paper fibers and the repulsion between particles would be influenced at the same time. On the one hand, the attraction between particles and fibers is reduced due to “the screening effect” from DLVO theory. On the other hand, the repulsion between particles is also reduced which probably lead to particle aggregation as well as the reduction of blocking effect (*32*). In our 80(+) particle elution experiments, the deposition appeared to increase when ionic strength was enhanced during elution (increase salt contents of paper). The possible reason for this is that high ionic strength caused particle aggregation and the reduction of the blocking effect (as shown in SEM and confocal results). Those effects counteracted the deposition loss due to attraction reduction between particles and paper fibers which lead to the increase of particle deposition.

3.3 Conclusions

(1) Latex surface potentials (mobilities) of particles are one of the main factors controlling particle deposition on paper fiber surfaces. More deposition was observed after particle with higher positive charge eluted in paper media and vice versa.

(2) Particle depositions retarded the elution flow and further reduce the elution distance

(3) No obvious influences of particle deposition and transportation when anionic latex elution flows with different velocities. Furthermore, the results of cationic particle elution shows that the particle deposition raised with increasing elution flow velocity.

(4) Increasing salt content on paper strips enhanced the particle deposition amounts of anionic particles during elution.

(5) The deposition of cationic particles formed a monolayer structure due to the "Blocking effect". However, increasing salt content in paper would reduce this blocking effect and further increase the particle deposition.

Chapter 4 Particle concentrated at the elution end as a result of evaporation

Abstract

In all the experiments described before, band shapes formed by concentrated particles at the elution end were always observed. This phenomenon was supposedly caused by the mass flow (MF_E), which occurred in order to refill the water loss due to evaporation. After the capillary flow reached the elution end, the suspended particles were carried continuously up to the elution end by MF_E and concentrated gradually. To theoretically describe the movement of this evaporation driven flow, a model was proposed and the predictions from the model fitted the experimental data well. Furthermore, the influences of evaporation on particle concentration were investigated. Based on our studies, a strategy was suggested to reduce sample loss during transportation in paper. Moreover, the effects of paper properties in liquid maximum elution distance on paper were studied by our model.

4.1 Particle concentrated during transportation in paper

Results

In order to understand the mechanisms that concentrate particles at the elution end, the influences of different evaporation rates on particle concentrating were studied. In these experiments, Allura Red (Sigma-Aldrich Cat No: 458848) (anionic) was eluted by paper strips. These strips were sealed with plastic bags in order to limit the water evaporation. In control experiments, paper strips without coverage were used. The elution was conducted at room temperature (around 25℃) with relative humidity around 45%. Details of this experiment were presented in chapter 2.3.4

Fig 4.1 showed the results of these experiments. After 1 hour of elution, Allura Red concentrating on the eluted end (top of eluted flow) of un-sealed paper strips was observed. However, there was no obvious concentration of dyes on those paper strips sealed with plastic bags. Furthermore, the elution distance of Allura Red solution in sealed paper strip is longer than that in strips without coverage.

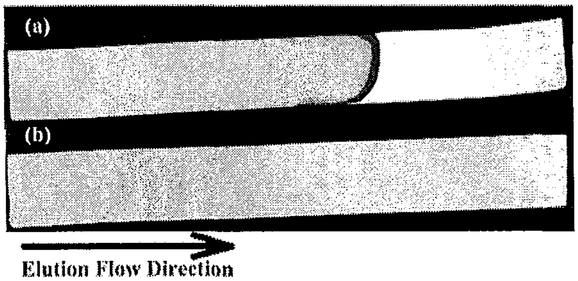

Figure 4.1 Images of paper strips after eluting Allura red for 1 hour in (a) atmosphere, and (b) evaporation limited environments (plastic sealed)

In order to understand how evaporation leads to the concentration of dyes and particles at the eluted end, the experiments of dyes eluted in wet paper strips were conducted. In these experiments, a series of black horizontal lines spaced out with 20 mm intervals were drawn across a long vertical strip of paper with water-insoluble ink (as shown in Fig 4.2). The first vertical black line followed by the series of black lines is either drawn 20 mm from the centre of the paper strip (strips (I) and (II)), or drawn 40 mm from one end of the paper strip (strips (III) and (IV)). Next, paper strips were submerged in deionized water to saturate the paper with water. Then, the Allura Red (anionic) dye was placed on the base black line on each saturated paper strip. Finally, the center of strip (I) was dipped into deionized water and the rest parts of paper strips were horizontally fixed above water for 30 min (The sketch is shown as follow (Fig 2.5(b)). Also, the bottom 10 mm of the strip (III) was dipped into deionized water for 30 min. Details of this experiment were shown in Chapter 2.3.4. Strips (II) and (IV) were placed horizontally and vertically for 30 min, respectively, as control groups. All the procedures in these experiments were conducted in atmosphere with the humidity around 45% (monitored by DRETEC hygrometer) and temperature around 25℃. Fig 4.2 showed the results of allura red movement in wet paper. Experiments using methylene blue (cationic) dyes were also done by following the same procedures. The results of methylene blue were shown in Fig 4.2 (b).

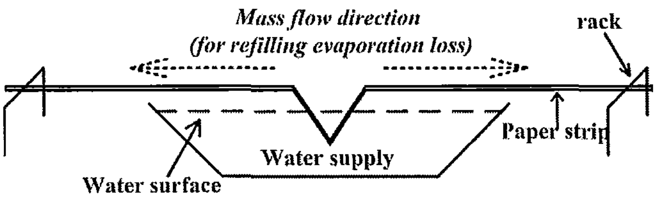

Recall: Fig 2.5 (b) Sketch of dye horizontal elution in water saturated paper strip

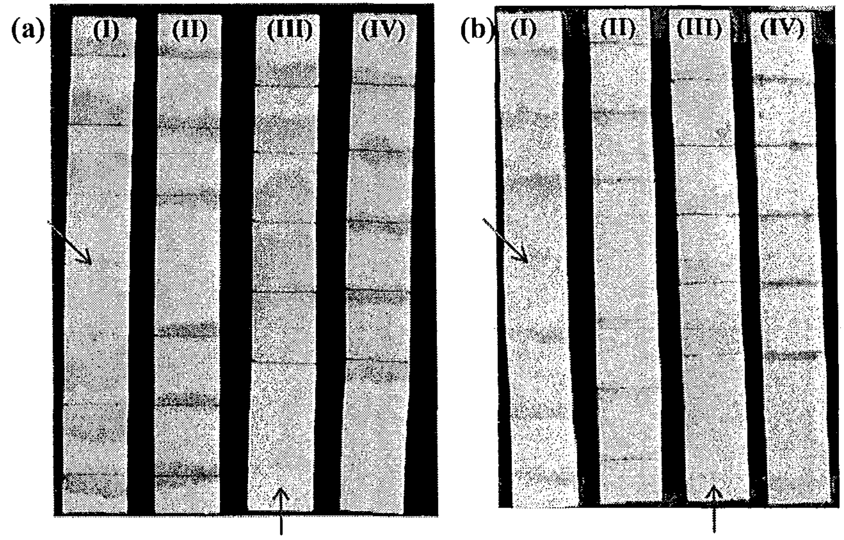

Figure 4.2 The transportation of (a) Allura Red and (b) methylene blue in wet paper with water supply at the (I) center and (III) the bottom (the sites of water supply were pointed by the arrows). In (II) and (IV), control groups without water supply were also set up.

Fig 4.2 (a) and (b) showed that both cationic and anionic dyes located on saturated paper strips were carried forward if the strips were partially dipped into water. The transport direction was away from the water supply. However, there was no obvious dye transportation on the strips of control groups (without water supply). These experimental data showed that there must be water flow migrating from the water supply towards the end of the paper strips that transports dyes away from the water supply. Furthermore, the dyes which were placed closer to the water supply would be transported longer than the dyes drawn farther.

Discussion

In many researches in latex film formulation (*74*), it was found that during the stage of water evaporation, particles will be brought close to packing latex films. Due to different evaporation rates on the latex film, more particles would concentrate at the "drying boundary" (which is the boundary between wet film and dry substrate) and make the edge of the latex film thicker (*75*). This is called the "coffee ring effect" first discovered by Deegan (*63*). Robert D. Deegan and coworkers suggested that in a droplet with a constant contact line with a solid substrate, liquid evaporating from the edge would be replenished by liquid from the interior. This edge-ward flow would carry dispersed materials to the edge and the dispersed materials will then concentrate to form the ring-like deposit that remains after all the liquid evaporates.

In our previous experiments in chapter 3, particles always concentrated at the eluted end in various circumstances such as different ionic strengths, different surface potentials, and different channel shapes. We believed these phenomena was also because of particles were transported and concentrated at the constant contact line (elution end). However, the mechanism that causes these phenomena is different from the coffee ring effect. In short, the coffee ring formation is caused by different evaporation rates in the center and edge of a liquid drop (*63*). However, in our research, the evaporation rate was assumed uniform on the whole surface area of paper if elution took place in constant humidity. Thus, there must be some factors other than evaporation rates that caused the particle concentration at the elution end of paper during all the experiments.

Fig 4.1 showed that the concentration of Allura Red didn't occur after elution in sealed paper strips. This phenomenon suggested that the concentration of particles at the eluted end was indeed caused by the evaporation of water in eluted latex on the paper strip. Therefore, once the evaporation was restricted, the concentration at the eluted end would not occur. Also, theoretically, the elution distance is controlled by the capillary force while no other external forces are applied. The earliest study of capillary force was conducted by Young and Laplace in the 19th century. The capillary force was given as:

$$F_c = 4\pi\gamma R\cos\theta \qquad \text{Eq (4.1.1)}$$

According to the above equation, the capillary force only depends on surface tension of the liquid (γ) and surface / liquid contact angle (θ), both of which are humidity independent. In each trial of our experiments in Fig 4.1, the same liquid (water) and capillary media (Whatman No.1 filter paper) were applied, which meant R (the pore radius) should be constant. Since the capillary force should not vary with evaporation, we can derive that the variation of elution distances in those experiments was due to other factors, which were dominated by evaporation.

Based on the mass balance, Fries et al. (*29*) have developed a model to describe the evaporation effect in capillary rise of water in porous media. Based on their work, a new model that describes the mass balance of water transportation in porous media can be established. First, the evaporation rate in the whole elution period is assumed constant and distributed uniformly. This assumption is valid when the evaporated moisture (water vapor) disperses rapidly, so the evaporation should not be retarded by the increase of moisture content, as well as when the heat source is uniformly distributed in the porous media. Fig 4.3 shows the illustration of the mass balance between the evaporation (M_E) and capillary (M_c) mass flow rate.

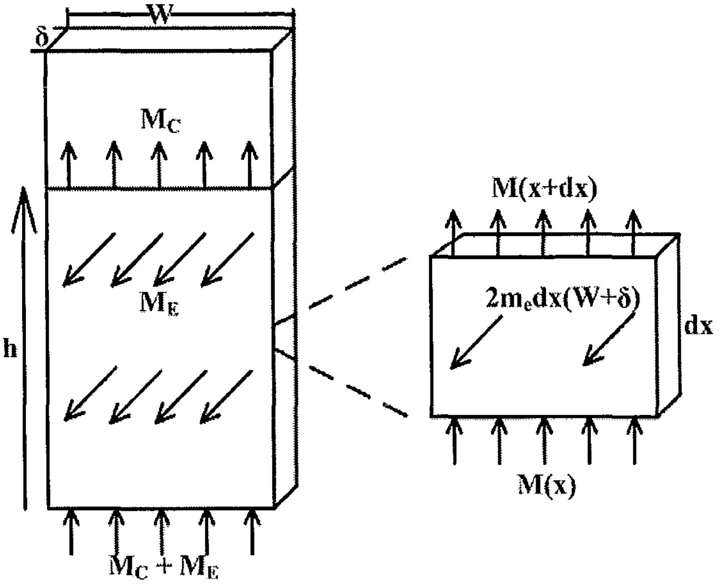

Figure 4.3 The illustration of the mass balance during water elution in paper (*29*)

M_c is given by:

$$M_C = dh/dt \times \rho \times A \qquad \text{Eq (4.1.2)}$$

where ρ(kg/m^3) is the density of water, *dh/dt* is the elution flow rate (mm/s) ,t is the elution time (s), and *A* means the vacancy cross sectional area of the paper strip (mm^2) (where water can flow through) which can be presented as δ (thickness of paper strip) x W (width of paper strip) x ϕ (porosity of paper strip). Next, evaporation is assumed to only occur on paper surfaces so that M_E can be presented as:

$$M_E = 2m_e \times h \times (W + \delta) \qquad \text{Eq (4.1.3)}$$

where m_e (Kg/m^2·s) is the constant evaporation rate and h is the elution distance (mm). By applying Eq(4.1.3), the differential mass balance (mass balance in a small distance dx) (Fig4.1.4) can be expressed as:

$$dM(x) = M(x + dx) - M(x) = -2m_e \times (W + \delta)dx \qquad \text{Eq (4.1.4)}$$

After integration of Eq (4.1.4) and applying the boundary condition that the mass flow rate in the beginning (x = 0) is $M_c + M_E$, the mass balance equation can be presented as:

$$M(x) = M_C + 2m_e \times (W + \delta) \times h \times (1 - \frac{x}{h}) \qquad \text{Eq (4.1.5)}$$

Once the elution flow reaches the eluted end, Mc will stop. On the other hand, M_E still takes place in order to refill the evaporation water until the paper strip leaves the water supply. Therefore, the mass flow rate in x becomes:

$$M(x) = 2m_e \times (W + \delta) \times h \times (1 - \frac{x}{h}) \qquad \text{Eq (4.1.6)}$$

By dividing *M (x)* with water density and vacancy cross sectional area (*A*), the velocity of mass flow after elution flow reaches the eluted end can be obtained as:

$$V_R(X) = M(x) / \rho A = 2m_e \times (W + \delta) \times h \times (1 - \frac{x}{h}) / \rho W \delta \phi \qquad \text{Eq (4.1.7)}$$

As shown in Eq 4.1.7, the maximum flow velocity takes place when $x = 0$ and can be expressed as:

$$V_{RMAX} = \frac{M_E}{\rho A} = \frac{2meh(W + \delta)}{\rho W \delta \phi} \qquad \text{Eq (4.1.8)}$$

Then substituting Eq 4.1.8 into Eq 4.1.7, the flow velocity can be presented as:

$$V_R(x) = V_{RMAX}(1 - \frac{x}{h}) \qquad \text{Eq (4.1.9)}$$

Eq (4.1.9) is able to explain the phenomenon in Fig 4.2 (a) and (b) that on wet paper strips, if the dyes were located closer to the water supply, it would be eluted longer than those drawn farther from the water supply. As afore mentioned, once the elution flow reaches the end position, the capillary flow would cease. However, since evaporation would still occur, the mass flow (MF_E) for refilling the evaporation loss would still take place until the paper strips were removed form the water supplies. In the results of Fig 4.1, since water evaporation continuously acted on paper strips exposed to the atmosphere, MF_E would keep taking place in those paper strips until the experiment stopped. Thus the dye particles would continue transporting to the eluted end. Finally, the band shapes of dye concentrations formed. On the contrary, there is no dye concentrating on evaporation limited paper strips. Therefore, a conclusion can be made that the formation of particle concentration at the elution end in our research was not due to different evaporation rates, but dominated by different flow rates of MF_E, which were varied with elution distances.

4.2 Influence of evaporation on particle concentration

Fig 4.4 shows the experimental and model simulation results of latex transported distances on paper during 1 hour of elution in different relative humidity levels. Calculation of model simulation results are presented in Appendix one. In Fig 4.4, it can be observed that the elution distance of latexes (cationic and anionic) would increase with the increase of relative humidity. The elution distances of cationic latex particles in 35 % humidity was much shorter (40 mm for 80(+) and 25 mm for 120(+)) than in 50 % or higher relative humidity (75 mm or higher for 80(+) and 60 mm or higher for 120(+)). In contrast, the increasing rate of elution distance was reduced after the relative humidity was higher than 50%. In Fig 4.4 (b), the significant change in anionic latex elution distances between 35% and 50 % can also be observed (50 mm to 85 mm). Nevertheless, there are significant differences in elution distances between 80(+) and 120(+) but not between two anionic latexes. Also when anionic latex was eluted in 100% humidity, both 60(-) and 135(-) particles reached the final end of the paper strips in 1 hour. So experimental results showed no differences in elution distances between 60(-) and 135(-) and no error bar is shown.

Figure 4.5 shows particle deposition of different latexes at the elution end after 1 and 2 hours of elution as a function of relative humidity. As observed in Fig 4.5, there are significant increases in particle depositions between 1 hour and 2 hours of elution at 35 % relative humidity (80(+):0.32, 120(+):0.12, 60(-):0.1, 135(-):0.15), and the increasing of particle deposition was diminished with the raise of relative humidity. When elution took place in 100% humidity, the particle concentration phenomenon could barely be observed. In summary, concentrated PS particles at the end of the elution path would be reduced by raised relative humidity.

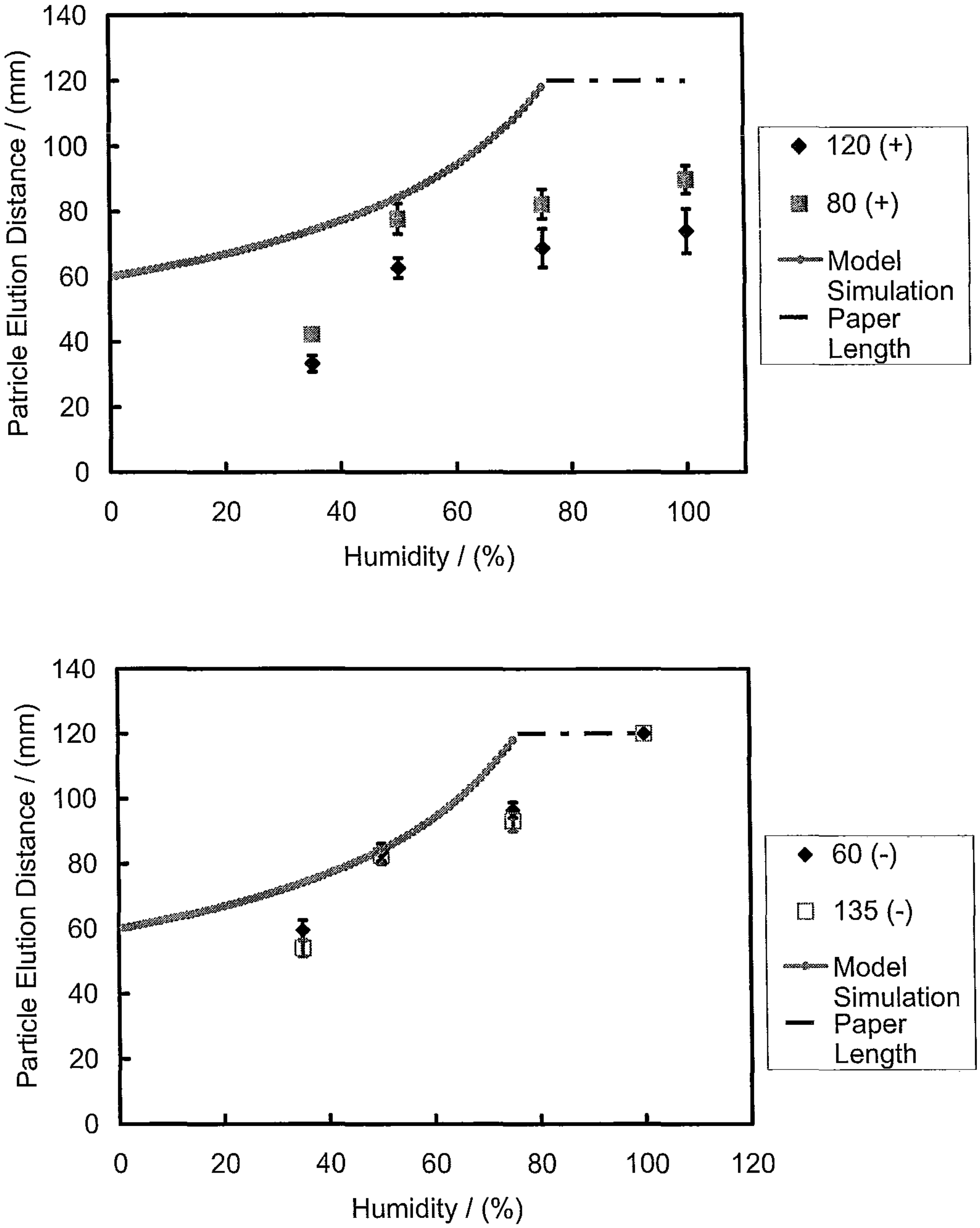

Figure 4.4 Experimental elution distance and model simulation of (a) cationic and, (b) anionic latexes after 1 hr elution in different surrounding humidity (since the length of paper strips in these experiments are 120 mm, the maximum of elution distances are 120 mm). The model simulation results are obtained by Eq. 4.2.11. The details of model calculation are presented in Appendix

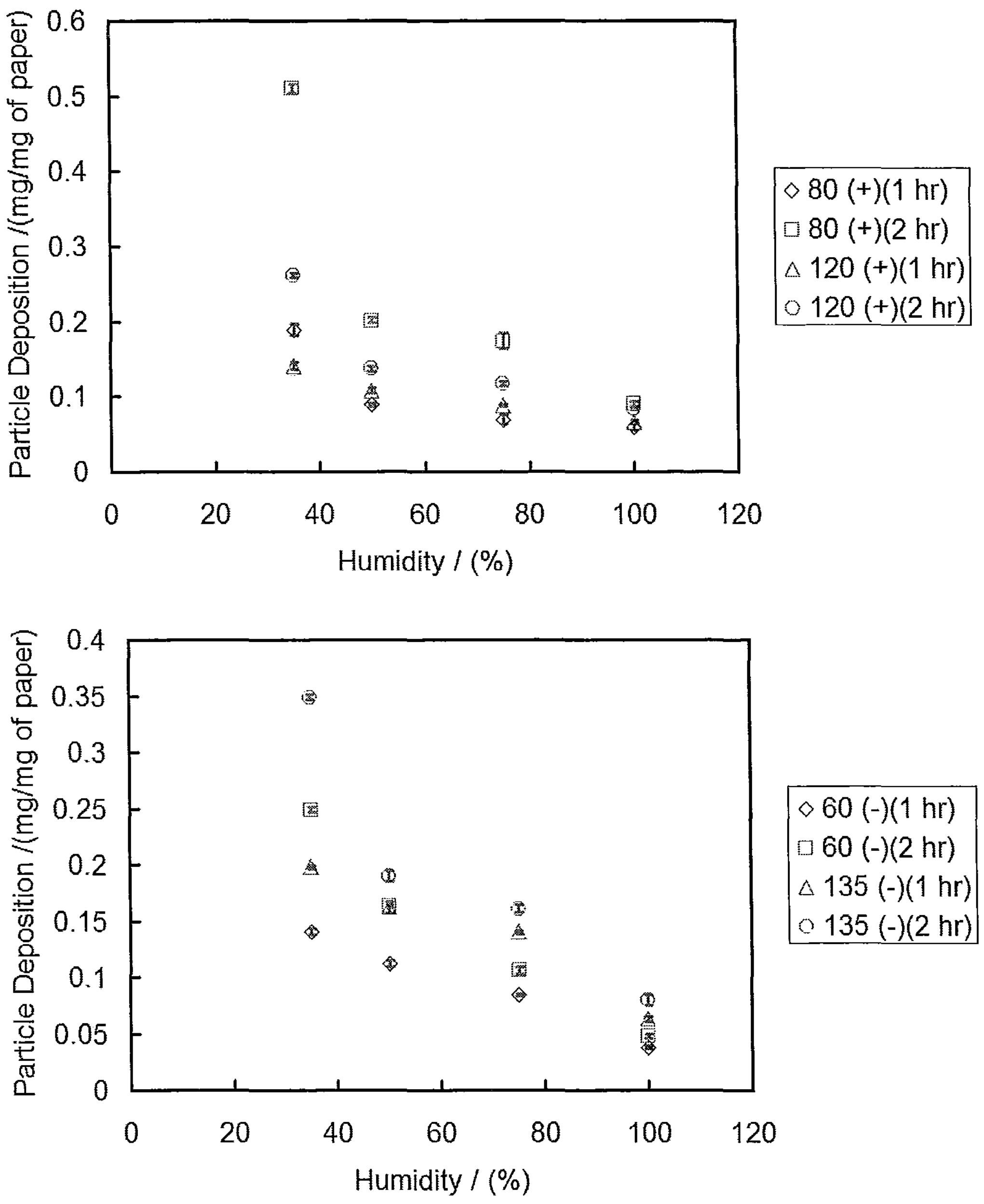

Figure 4.5 Particle deposition of (a) cationic and (b) anionic latexes at eluted end of paper (where the concentration of particles took place) after 1 hour and 2 hours elution as a function of relative humidity

Fig 4.6 (a) shows the cross section fluorescence images in paper strips, which eluted 135(-) for 1 hr in atmosphere (humidity is around 45%). It can be observed that after the paper strips were dried, most particles deposited on the surface of paper, and only a few particles trapped by paper fibers remained inside the paper strip. Furthermore, in Fig 4.6 (b), 80(+) particles were eluted for 1 hr in atmosphere (relative humidity around 50%); it can be observed that deposited particles formed a mono layer like structure on the fiber surface. However, a particle deposition layer is also observed on the paper surface.

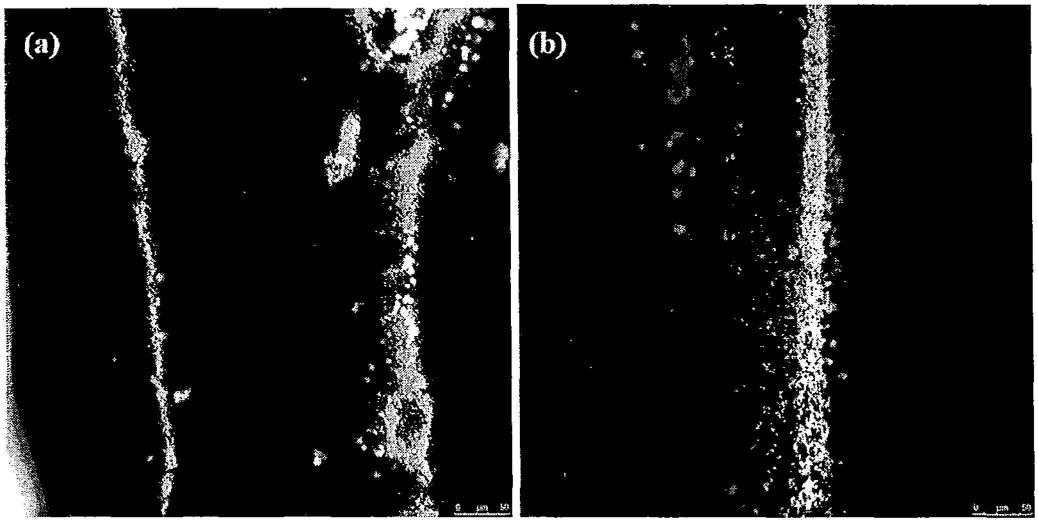

Figure 4.6 Cross section fluorescence images in paper strip after eluted (a) 135 (-), and (b) 80 (+) latexes. The bright layer is the fluorescence emitted from the latex particles, which mostly deposited on paper surface.

Consequently, in order to suggest a strategy for diminishing the sample losses during transport in paper porous media, the experiments with partially reduced evaporation rates were done. As we can observe in Fig 4.7 (a), less dye was deposited in the region covered by plastic strips. The plastic strips were used to reduce the evaporation rate in that region. Moreover, Fig 4.7 (b) shows images and particle deposition amount of 80(+) latex eluted through the paper strip with plastic strips covered in the middle. The results showed that particle deposition at the region of restricted evaporation rate was smaller than the one with normal evaporation which indicated that the amount of particle deposition was also diminished.

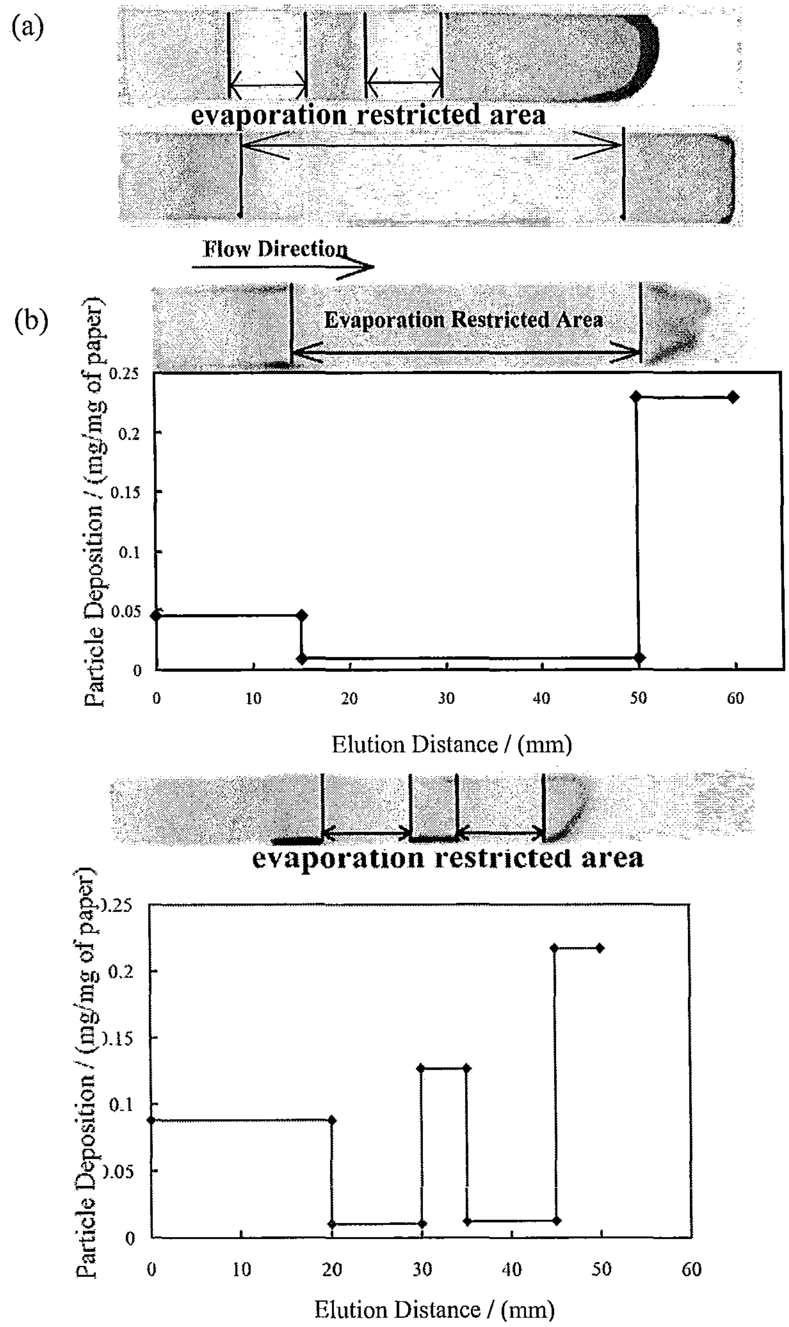

Figure 4.7 (a) 1 hour elution of Allura red in paper strips covered by plastic strips (between two black lines), (b) Images (black white inverted) and particle deposition amount of 1 hr elution of 80(+) in paper strips partially covered by plastic strips

Discussion

Fries *et al.* (*29*) suggested an equation for describing momentum balance of capillary liquid flow in porous media which includes the influences caused by evaporation:

$$p_c = p_h + p_{h(t)} + p_R \qquad \text{Eq (4.2.1)}$$

Where P_c is capillary ($P_c = 2\sigma\cos\theta / Rs$ (Rs is capillary radius, 7.6 μm for Whatman No.1), P_h is gravity (ρgh), $P_{h(t)}$ is the viscous pressure loss of capillary mass flow (Mc), and P_R is the viscous pressure loss of mass flow to replenish evaporation loss (M_E). Furthermore, the viscous pressure loss can be calculated as:

$$p_{h(t)} = \frac{\phi}{k}\mu\int_0^h h(t)dx = \frac{\phi}{k}\mu h \cdot h(t) \qquad \text{Eq (4.2.2)}$$

$$p_R = \frac{\phi}{k}\mu\int_0^h \upsilon_R(x)dx = \frac{\phi}{k}\mu\frac{1}{2}h\upsilon_{RMAX} \qquad \text{Eq (4.2.3)}$$

Substitute Eq (4.2.2) and Eq (4.2.3) into Eq (4.2.1), the momentum balance becomes:

$$\frac{2\sigma\cos\theta_s}{R_s} = \rho gh + \frac{\phi}{k}\mu h \cdot h(t) + \frac{\mu m_e(W+\delta)}{k\rho W\delta}h^2 \qquad \text{Eq (4.2.4)}$$

Eq 4.2.4 can be transformed to:

$$h(t) = \frac{a}{h} - b - ch \qquad \text{Eq (4.2.5)}$$

Then, three coefficients a, b, and c can be defined as follows:

$$a = \frac{2\sigma\cos\theta_s}{\phi\mu}\frac{K}{R_s} \qquad \text{Eq (4.2.6)}$$

$$b = \frac{\rho gK}{\phi\mu} \qquad \text{Eq (4.2.7)}$$

$$c = \frac{m_e(W+\delta)}{\rho W\delta\phi} \qquad \text{Eq (4.2.8)}$$

Where K represents the permeability (m^2) and can be obtained by experiment as described in Chapter 2.2 by measuring h(t) and t during water elution by Whatman No 1 filter paper. $\cos\theta_s$ is the contact angle between paper and water which is assumed to be 1 based on Liukkonen's (*76*) research. Liukkoen suggested that the contact angle of α-cellulose is 0 and Whatman No.1 is composed of 98% α-cellulose. Furthermore, m_e can be calculated by the equation suggested in ASHRAE handbook (*77*):

$$m_e = (Pw - Pa) \times (0.089 + 0.0782 V_{air}) / Y \qquad \text{Eq (4.2.9)}$$

where Pw is the saturated water vapor pressure (kPa), Pa is the partial pressure of water vapor (kPa), V_{air} is the air flow velocity in the environment which is assumed to be zero in these experiments, and Y is the heat of vaporization of water which is 2257 kJ/Kg.

Therefore c can be present as:

$$c = \frac{3.94 \times 10^{-5} (Pw - Pa)(W + \delta)}{\rho W \delta \phi} \qquad \text{Eq (4.2.10)}$$

Moreover, by setting h(t) equal to 0, the maximum height can be obtained:

$$h_{\max,a,b,c} = \frac{-b}{2c} + \sqrt{\frac{b^2}{4c^2} - \frac{a}{c}} \qquad \text{Eq (4.2.11)}$$

By Eq 4.2.11, we can derive that h_{maz} is inversely proportional to c which is the evaporation rate coefficient. According to Eq 4.2.10, water in an environment with lower water vapor pressure (lower humidity) would have higher evaporation rate. Therefore, the capillary eluted distance would decrease when elution occurs in environment with high relative humidity. This derivation agrees with results shown in Fig 4.4. The elution distances of particles are the shortest while elution was conducted in lowest (35%) humidity; nevertheless, elution distances increased when humidity levels rose.

Experimental results of latex elution distances were also fit by the model developed before (Eq 4.2.11). The fitting results showed that there are about 2 - 15% discrepancies between experimental elution distances of anionic latex and model simulations. Fries *et al.* (*29*) suggested that the discrepancies are due to the higher evaporation rate on the wicking top (capillary flow front). The discrepancies may be also due to the wind flow during elution experiments, which was assumed 0 m/s in the model calculation. However, if the wind flow velocity was assumed 0.15 m/s (the minimum wind flow in nature) in model calculation, the maximum discrepancy would be reduced to 13 %. This is shown in the following figure (Fig 4.8).

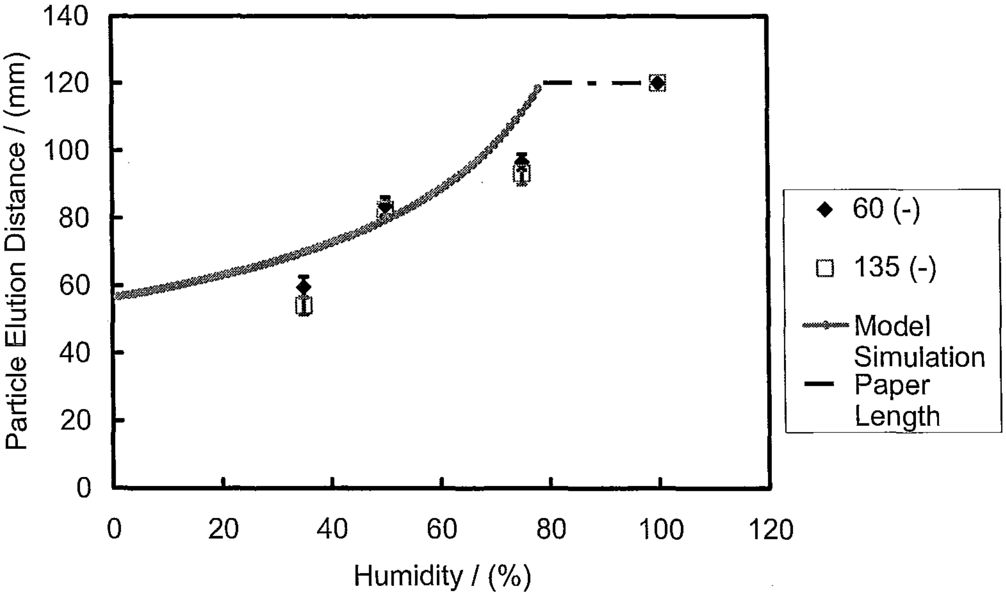

Figure 4.8 Experimental elution distance and model simulation of (a) cationic and, (b) anionic latexes after 1 hr elution in different surrounding humidity with wind flow velocity 0.15 m/s. The model simulation results are obtained by Eq. 4.2.11. The details of model calculation are presented in Appendix

Moreover, there are stronger discrepancies (10-50 %) that can be observed when fitting cationic latex elution distances where the model calculation of maximum elution distances is higher than experimental results. According to the experimental results presented in Chapter 3.1 (Table 3.1), we suggest that the increase of discrepancies is because of the retardation of liquid penetration by particle deposition. This retardation of liquid penetration further reduces the maximum elution distance.

In the chapter 4.1, it was suggested that there was a mass flow (MF_E) which occurred in the whole elution period in order to refill the evaporation loss of water. Besides, MF_E would transport dyes and cause the concentration of dyes at the eluted end. This phenomenon can also be obtained in experiments results shown in chapter 3 (Fig 3.1, Fig 3.5, Fig 3.6, and Fig 3.3.1) where particles concentrated at the end of elution and formed a band shape. Since MF_E was driven by the evaporation loss of water, once evaporation diminished, the flow rate of M_E should also decrease. Thus, the flow rate of MF_E would be lower in an environment with higher humidity (lower evaporation rate). As seen in Fig 4.5, by comparing the differences of particle deposition between 1 hour and 2 hours of elution in different humidity, the diminishing of MF_E caused by higher evaporation rate can be obtained. During elution in 35% of relative humidity, obvious concentration took place regardless of differences in surface charge and particle size. The concentration phenomenon decreased along with the raise of relative humidity.

Our experimental results also show that during elution, particles at the center of paper (where is no evaporation) are not only transported further by the elution flow, but also transport outward to the paper surface in order to refill the liquid loss due to evaporation. This outward transportation of particles would continue to take place until the paper strips were completely dry which caused most suspended particles (particles which were not fixed on to paper fibers) to move to the paper surface. This phenomenon is clearly observed in Fig 4.6 where particles were transported towards the paper surface during and after elution which formed a deposition layer on the paper surface. These results show that the particle concentration phenomenon also takes place in the direction perpendicular to elution flow.

When applying paper analytical devices, getting large amount of samples in the sensing area is sometimes required to obtain higher signal intensity. We can achieve that by controlling the evaporation rate. As results observe in Fig 4.7, we are able to reduce the amount of particle deposition by diminishing the evaporation rate. We believe this phenomenon occurred once solutions eluted in paper strips have different regions of evaporation rate; solution would tend to flow towards region with higher evaporation rate in order to refill lost liquid. Therefore, more particles would be brought to those regions and deposited there. So, if we diminish the evaporation during particles elution, fewer particles would be lost during transportation and more particles would finally concentrate in the eluted end.

4.3 Model analysis on factors influencing the maximum elution distance

Paper properties are considered as some of the most important factors that influence liquid (and colloid) movement during elution. According to Eq 4.2.11, there are three variables (*a, b*, and *c*) that influence the maximum elution distance, and the three variables are dominated by different paper properties:

$$h_{\max,a,b,c} = \frac{-b}{2c} + \sqrt{\frac{b^2}{4c^2} - \frac{a}{c}} \qquad \text{Eq (4.2.11)}$$

where *a, b,* and *c* are

$$a = \frac{2\sigma\cos\theta_s}{\phi\mu}\frac{K}{R_s} \qquad \text{Eq (4.2.6)}$$

$$b = \frac{\rho g K}{\phi\mu} \qquad \text{Eq (4.2.7)}$$

$$c = \frac{m_e(W+\delta)}{\rho W\delta\phi} \qquad \text{Eq (4.2.8)}$$

The relevant paper properties include: θ_s (contact angle), ϕ (porosity), K (permeability), Rs (capillary radius (pore radius)), W (width), and δ (thickness). Moreover, μ is the liquid viscosity, σ is the surface tension of the liquid and d is the liquid density. We applied deionized water in the calculation as eluted liquid and assumed those properties were constant during elution. (Deionized water properties: Viscosity (μ): 8.49×10^{-4} (Pa·s), Density (d): 1 (kg/L), and Surface tension (σ): 67.91 (kg/s^2)). Also, all the simulations are based on a relative humidity of 50 %.

The influences of thickness, porosity, and contact angle on maximum water elution distance were simulated by our model. The influence of each property on elution was estimated separately with the others kept constant. Simulation results of maximum elution distance as a function of different varying paper properties are shown in the following paragraphs, respectively.

4.3.1 Paper thickness

Fig 4.8 shows the simulation result of maximum water elution distances (h_{MAX}) on paper strips (Whatman No. 1) with different thicknesses. In general, elution distances increase with the increase of paper thicknesses. It can be observed that the h_{MAX} increases from 63 to 188 mm when the thickness increases from 0.1 to 1 mm. Furthermore, the influence of thickness on h_{MAX} is strong when the thickness changes from 0.1 to 0.5 mm. When the thickness of paper increases 0.1 mm, h_{MAX} increases from 13 to 20 mm. Moreover, this enhancement effect of h_{MAX} diminishes as the paper thickness increases. Simulation in paper thickness between 0.5 to 1 mm shows that h_{MAX} rises 8 to 11 mm when thickness increases every 0.1 mm. In thicknesses between 1 to 2 mm, h_{MAX} would increase 67 mm which is a 6.7 mm increase in elution distance for every 0.1 mm increase in thickness on average.

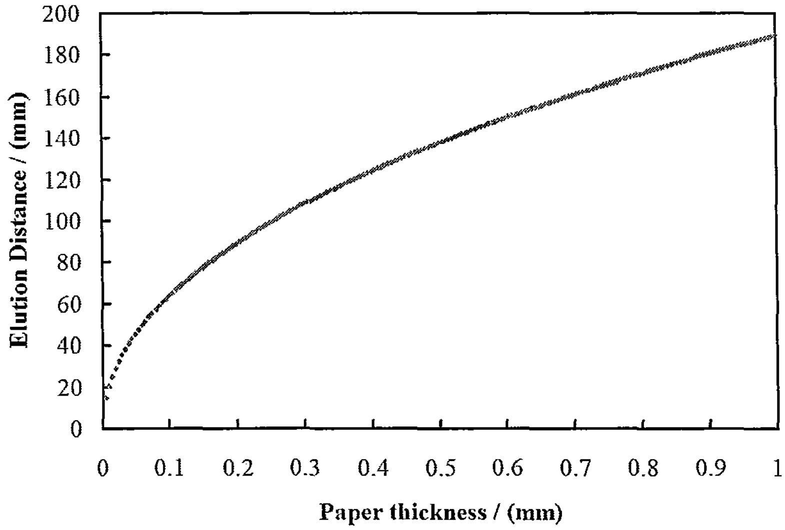

Figure 4.9 Simulation results of deionized water maximum elution distance in paper (Whatman No. 1) with thickness 0-1 mm (other properties of paper: Width (W): 0.02 (m), Porosity (ϕ): 0.7422, Average capillary radius (Rs): 7.609×10^{-6} (m), Permeability (K): 0.131×10^{-12} (m^2) and Contact angle (θs): 0°)

According to Eq 4.1.7 and Eq 4.1.8, we can conclude that the increase in paper thickness would reduce $V_R(x)$, which is the flow velocity of MF_E (mass flow for refill evaporation loss). Furthermore, based on Eq 4.2.1 and Eq 4.2.4, reduction of $V_R(x)$ would further decrease P_R which is pressure loss due to MF_E. The decrease of P_R suggests that the influence of evaporation on mass flow is getting weak when the thickness of paper increases. Nevertheless, since one source of pressure loss (P_R) is reduced, liquid would be able to travel farther. To sum it up, the increase of paper thickness would enhance h_{MAX}. Eq 4.1.7, Eq 4.1.8, Eq 4.2.1 and Eq 4.2.3 are recalled as follows:

$$V_R(X) = M(x)/\rho A = 2m_e \times (W+\delta) \times h \times (1-\frac{x}{h})/\rho W\delta\phi \qquad \text{Eq (4.1.7)}$$

$$V_{RMAX} = \frac{M_E}{\rho A} = \frac{2meh(W+\delta)}{\rho W\delta\phi} \qquad \text{Eq (4.1.8)}$$

$$p_c = p_h + p_{h(t)} + p_R \qquad \text{Eq (4.2.1)}$$

$$p_R = \frac{\phi}{k}\mu\int_0^h \upsilon_R(x)dx = \frac{\phi}{k}\mu\frac{1}{2}h\upsilon_{RMAX} \qquad \text{Eq (4.2.3)}$$

4.3.2 Pore Size

Fig 4.9 shows the simulation result for the maximum deionized water elution distances (h_{MAX}) in paper (Whatman No. 1) with different pore sizes (capillary radius). In general, h_{MAX} would decrease if the pore size increases. The capillary force in our model is calculated by Young-Laplace equation. According to this equation, increasing the capillary radius would decrease the capillary pressure and further result in reduced travel distances. Furthermore, as shown in this simulation, the effect of pore size on h_{MAX} is significant for pore sizes from 0 to 2 μm (th_{MAX} would consequently decrease from 753 mm to 168 mm). Then this effect becomes gentle when pore size increases from 2 to 10 μm: from 2 to 4 μm, h_{MAX} reduces around 2 mm with every 0.1 μm increase; from 4 to 7 μm h_{MAX} reduces around 1 mm with every 0.1 μm increase; and from 7 to 10 μm h_{MAX} reduces around 0.5 mm with every 0.1 μm increase.

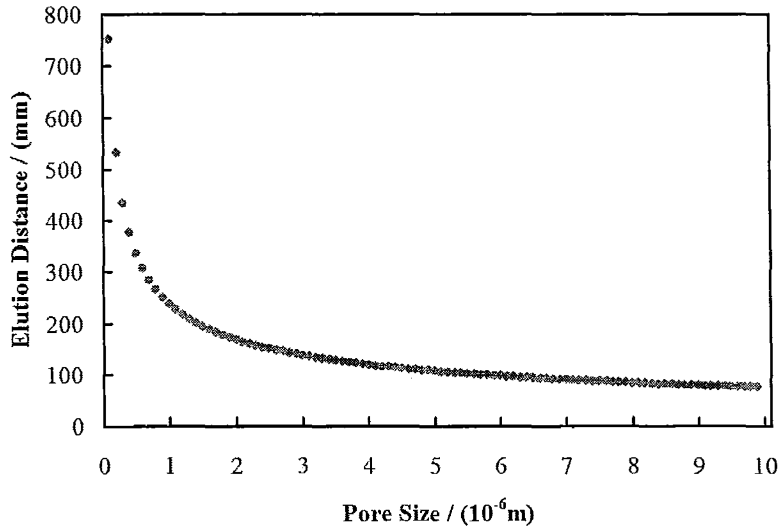

Figure 4.10 Simulation results of deionized water maximum elution distance in paper (Whatman No. 1) with pore size (capillary radius (Rs)) 0-10 μm (other properties of paper: Width (W): 0.02 (m), Thickness (δ) 180 μm, Porosity (ϕ): 0.7422, Permeability (K): 0.131 $\times 10^{-12}$ (m^2) and Contact angle (θs): 0°)

4.3.3 Permeability

Fig 4.10 is the simulation result of h_{MAX} in paper strips with different permeabilities (K). In general, h_{MAX} would increase with the raise of paper permeabilities. Paper permeability in this research was obtained by calculation with the experimental data of h (elution distance) and t (elution time) relationship. The calculation of K is based on the equation suggested by Fries *et al.* (29):

$$h^2 = \frac{4\sigma\cos\theta_s}{\phi\mu}\cdot\frac{K}{Rs}\cdot t \qquad \text{Eq 2.2.1}$$

This equation shows that K is proportional to the flow velocity (h/t) if other parameters of paper are kept constant. This suggests that K would increase with an increase in capillary flow velocity; nevertheless, raising flow velocity would further lead to the enhancement of h_{MAX}. Furthermore, the simulation result also shows that the relationship between h_{MAX} and K becomes linear after permeability reaches a value higher than 0.1 which suggests that the effect of K in h_{MAX} diminishes after K is larger than 0.1.

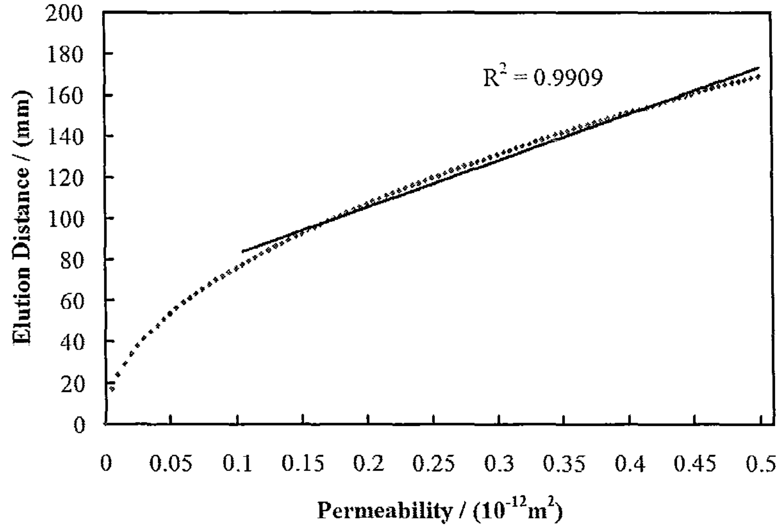

Figure 4.11 Simulation results of maximum deionized water elution distance in paper (Whatman No. 1) with permeability 0-0.5 ($\times 10^{-12}m^2$) (other properties of paper: Width (W): 0.02 (m), Thickness (δ) 180 μm, Average capillary radius (Rs): 7.609×10^{-6} (m), Porosity (ϕ): 0.7422, and Contact angle (θs): 0°)

Note:

Before simulating the influence of elution distance cause by porosity and contact angle, it has to emphasized that paper permeability (K) in this research is obtained by calculation which is based on Eq 2.2.1 suggested by Fries *et al.* (*29*). The equation shows that K is proportional to porosity (ϕ) and inversely proportional to $\cos\theta_s$ (cosine contact angle). In the following simulation, K is assumed constant ($K=1.037\times10^{-7}$ mm^2 (Whatman No. 1)). However, in a real situation, K may also vary with porosity and the contact angle of paper.

4.3.4 Porosity

According to Eq 4.2.6, Eq 4.2.7, Eq 4.2.8, and Eq 4.2.11, it can be observed that three parameters a, b, and c are all inversely proportional to porosity (ϕ). Therefore, we can derive that porosity should be given away in the calculation of maximum elution distance. However, as mentioned before, paper permeability (K) is proportional to porosity which suggested that the increase of porosity may lead to an increase in permeability and further enhance the maximum elution distance.

4.3.5 Contact Angle

The simulation result of maximum deionized water elution distances in paper (Whatman No. 1) with different contact angles is shown in Fig 4.11. The simulation shows that the maximum elution distance of liquid would decrease if the contact angle of paper increases. As mentioned in Chapter 4.3.2, capillary force in our model is calculated by Young-Laplace equation. According to Young-Laplace equation, capillary pressure is proportional to $\cos\theta s$ (cosine contact angle) and $\cos\theta s$ keeps decreasing when θs varies from 0°-90°. Consequently, it can be derived that the varying of θs from 0°-90° would reduce the maximum elution distance of liquid which is confirmed by the simulation result. Furthermore, the simulation result shows that when paper is really hydrophilic (θs<30°), the influence of contact angle on maximum elution distance (h_{MAX}) is small (h_{MAX} decrease from 86 to 80 mm). Once paper becomes more hydrophobic (θs increasing), the influence of the contact angle on h_{MAX} gets stronger (h_{MAX} decreases to 60 mm when the contact angle is 60°; 36mm when the contact angle is 80°). In short, h_{MAX} of liquid is higher when liquid is eluted in more hydrophilic paper. Moreover, as mentioned before, paper permeability (K) is inversely proportional to $\cos\theta s$. Thus, decreasing of $\cos\theta s$ (increasing of θs) may also lead to the increase of permeability and further diminishes the effect of θs on h_{MAX}.

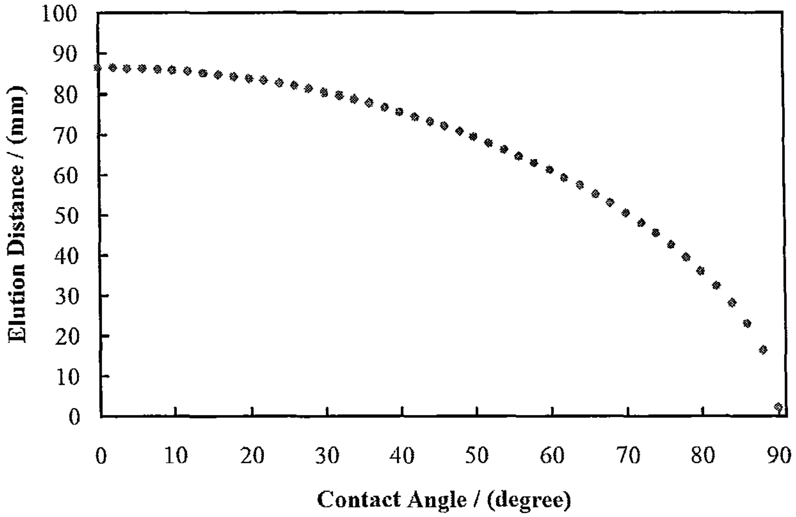

Figure 4.12 Simulation results of maximum deionized water elution distance in paper (Whatman No. 1) with Contact angle (θs) 0°-90° (other properties of paper: Width (W): 0.02 (m), Thickness (δ) 180 μm, Porosity (ϕ): 0.7422, Permeability (K): 0.131 $\times 10^{-12}$ (m^2) and average capillary radius (Rs):7.609$\times 10^{-6}$ (m))

4.3.6 Overall influence and Conclusion

Fig 4.12 shows the simulation result of maximum deionized water elution distance (h_{MAX}) as a function of relative humidity (1% - 95%) when elution occurs in paper with varying parameters, respectively. The effect of relative humidity from 96% to 100% is too strong and would overlap the influence of other factors. Thus, the simulations are conducted only in the range of 1%-95% relative humidity. In Fig 4.12, it can be observed that there is no effect of decreasing half porosity on h_{MAX} which is suggested in Chapter 4.3.4. Moreover, h_{MAX} is the most sensitive to pore radius in comparison to the other parameters. Furthermore, the effects of half thickness and half permeability are about the same on h_{MAX}. In conclusion, the rank of effects caused by paper parameters on h_{MAX} from high to low is: pore radius (capillary radius (Rs)) > permeability (K) ≒ thickness (δ) > contact angle (θs) >> porosity (ϕ) (no effect).

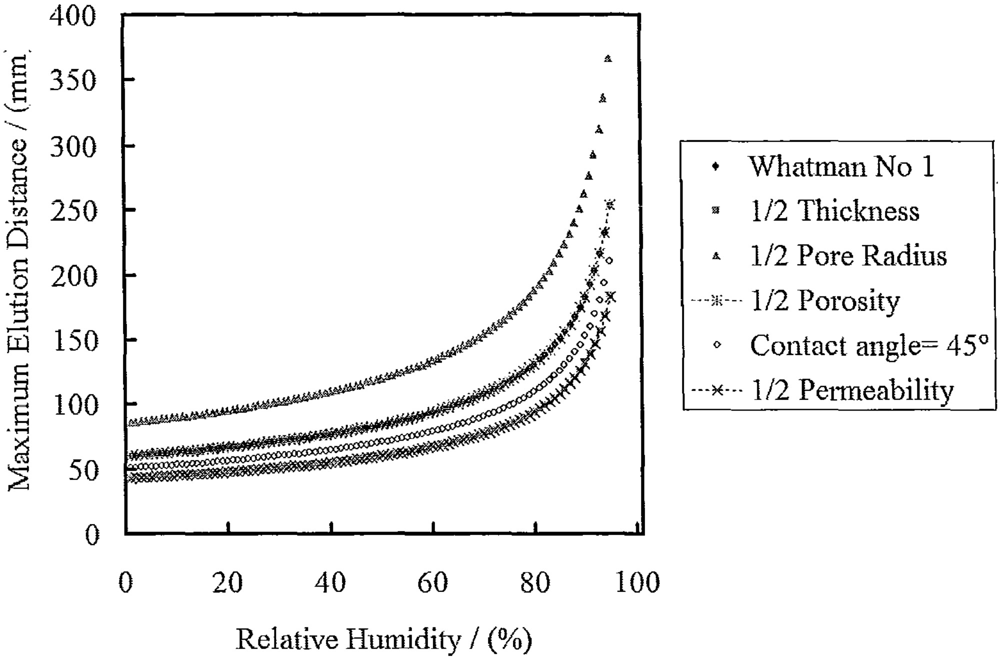

Figure 4.13 Simulation results of deionized water maximum elution distances in paper with varying parameters (½ thickness (δ), ½ pore radius (Rs), ½ porosity (ϕ), ½ permeability (K) and 45° contact angle (θs)) as a function of RH (1% - 95%). The varying parameter is listed beside figure. Other constant paper parameters is applied the properties of Whatman No 1 in simulations.

Chapter 5 Conclusions

According to the experimental results and theoretical discussions the following conclusions can be made.

(1) Latex surface potentials (mobilities) of particles are one of the main factors controlling particles deposition on paper fiber surfaces. More deposition was observed when particles with positive charge (than negative) eluted in paper and vice versa.

(2) Particle depositions retard the elution flow and further reduce the elution distance.

(3) No obvious influences of particle deposition when anionic latex elution flows with different velocities. Furthermore, the results of cationic particle elution shows that the particle deposition raised with increasing elution flow velocity.

(4) Increasing salt content on paper strips enhances the particle deposition amounts of anionic particles during elution.

(5) The deposition of cationic particles formed a monolayer structure due to the "Blocking effect". However, increasing salt content in paper reduced this blocking effect and further increases the particle deposition.

(6) The formation of particle concentration at the elution end in this research is not due to different evaporation rates, but dominated by MF_E which occurred in order to refill the water loss due to evaporation.

(7) The maximum elution distance (h_{MAX}) is strongly related to relative humidity. The lower h_{MAX} occurs in higher relative humidity.

(8) MF_E also takes place in the direction perpendicular to elution flow which transported particles outward to the paper surface to refill the evaporative loss on the surface. Experimental results show a particle concentration layer (bright layer in Fig 4.6) formed on paper surface after the paper was completely dried.

(9) The experimental results show that the amount of particles deposited when latex solutions eluted through paper strips is reduced in diminishing evaporation rate areas. Thus, we suggest that if the evaporation is limited during samples transported in paper analytical devices, the sample lose caused by deposition on paper fibers can be diminished.

(10) According to the model simulations (Eq 4.2.11), the rank of effects caused by paper parameters on h_{MAX} from high to low is: pore radius (capillary radius (Rs)) > permeability (K) ≒ thickness (δ) > contact angle (θs) >> porosity (ϕ) (no effect).

Appendix: Model calculation of the elution distance

Constant Parameters

Temperature: 25℃

Water saturated pressure at 25℃ (P_w): 3170 (Kg/(m*s^2))

Whatman No 1 paper strips

Width (W): 0.02 m

Average thickness (δ): 1.8 x10^{-4} m

Porosity (ϕ): 0.7422 (porotech co.)

Average capillary radius (Rs): 7.609x10^{-6} m (porotech co.)

Permeability (K): 0.131 x10^{-12} m^2

Contact angle (θs): 0° (Liukkonen, 1997)

Deionized Water

Viscosity (μ): 8.49x10^{-4} Pa*s

Density (dw): 1kg/L

Heat of vaporization of water (Y): 2257 KJ/Kg

Varying Parameters

Relative Humidity (RH): 35%, 50%, 75%, 100%

Water partial pressure (P_{RH}): RHx3170 (Kg/(m*s^2))

Calculation procedures

(1) The evaporation rate of water at each RH can be calculated by:

$$m_e = (P_w - P_{RH}) \times (0.089 + 0.0782 V_{air}) / Y \qquad \text{Eq (4.2.9)}$$

(from ASHRAE handbook edition 2003)

where V_{air} is 0 m/s, and the evaporation rate of water at four (or more) different RHs can be obtained as following:

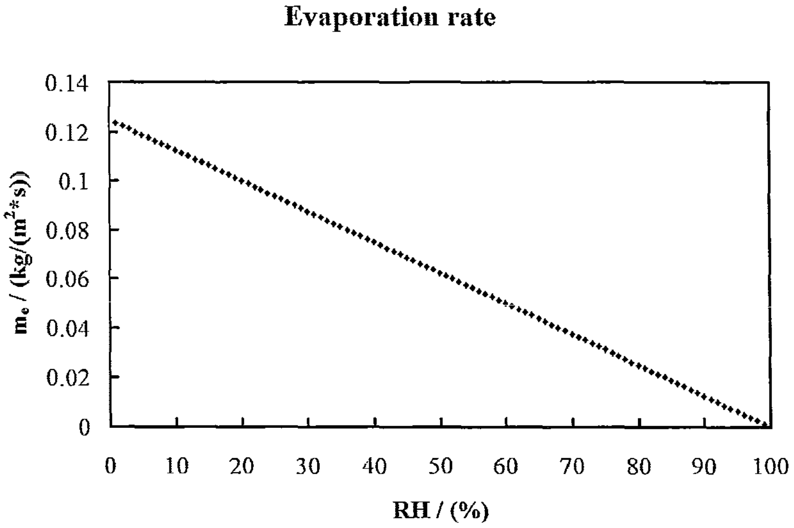

(2) The maximum height that water capillary flow can reach in paper is calculated by:

$$h_{\max,a,b,c} = \frac{-b}{2c} + \sqrt{\frac{b^2}{4c^2} - \frac{a}{c}} \qquad \text{Eq (4.2.11)}$$

Where a, b and c is

$$a = \frac{2\sigma \cdot K}{\phi \mu R_s} = 3.517 \times 10^{-6} \frac{m^2}{s}, b = \frac{\rho g K}{\phi \mu} = 1.932 \times 10^{-6} \frac{m}{s} \text{ and } c = \frac{m_e (W + \delta)}{\rho \cdot W \cdot \delta \cdot \phi}$$

We can see that c is a function of m_e, and then c at different m_e can be calculated.

(3) Consequently, by substituting a, b, and c into Eq (4.2.11), h_{max} at different RHs can be obtained as following:

Elution Distance at different RH (Whatman No. 1)

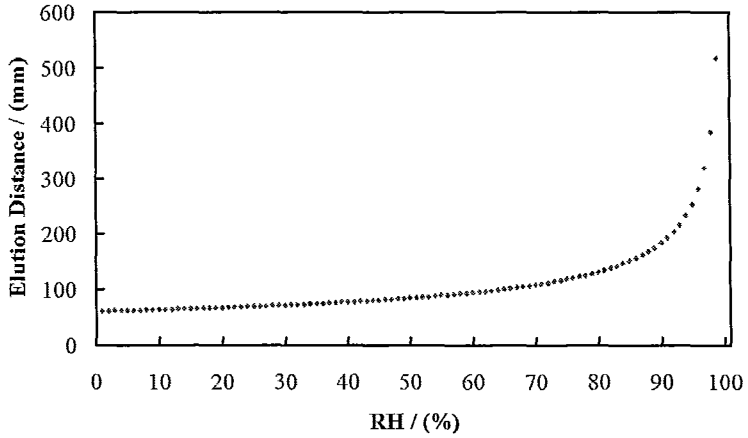

References

1. W.C. Bliesner. (1963) in Ph.D. Thesis:A study of the porous structure of fibrous sheets using permeability techniques, The Institute of Paper Chemistry, Lawrence College,Appleton, Wisconsin.
2. D.H. Horstmann, J.D. Lindsay, and R.A. Stratton. (1991) Using edge-flow tests to examine the inplane anisotropic permeability of paper, ***Tappi J.*** *74*,(4), 241-247.
3. W.A. Zhao, and A. van den Berg. (2008) Lab on paper, ***Lab on a Chip*** *8*,(12), 1988-1991.
4. Z.H. Nie, C.A. Nijhuis, J.L. Gong, X. Chen, A. Kumachev, A.W. Martinez, M. Narovlyansky, and G.M. Whitesides. Electrochemical sensing in paper-based microfluidic devices, ***Lab on a Chip*** *10*,(4), 477-483.
5. R. Pelton. (2009) Bioactive paper provides a low-cost platform for diagnostics, ***Trac-Trends in Analytical Chemistry*** *28*,(8), 925-942.
6. A.W. Martinez, S.T. Phillips, G.M. Whitesides, and E. Carrilho. Diagnostics for the developing world: Microfluidic paper-based analytical devices, ***Analytical Chemistry*** *82*,(1), 3-10.
7. D.A. Bruzewicz, M. Reches, and G.M. Whitesides. (2008) Low-cost printing of poly(dimethylsiloxane) barriers to define microchannels in paper, ***Analytical Chemistry*** *80*,(9), 3387-3392.
8. A.W. Martinez, S.T. Phillips, B.J. Wiley, M. Gupta, and G.M. Whitesides. (2008) Flash: A rapid method for prototyping paper-based microfluidic devices, ***Lab on a Chip*** *8*,(12), 2146-2150.
9. Y. Lu, W.W. Shi, L. Jiang, J.H. Qin, and B.C. Lin. (2009) Rapid prototyping of paper-based microfluidics with wax for low-cost, portable bioassay, ***Electrophoresis*** *30*,(9), 1497-1500.
10. K. Abe, K. Suzuki, and D. Citterio. (2008) Inkjet-printed microfluidic multianalyte chemical sensing paper, ***Analytical Chemistry*** *80*,(18), 6928-6934.
11. A.W. Martinez, S.T. Phillips, M.J. Butte, and G.M. Whitesides. (2007) Patterned paper as a platform for inexpensive, low-volume, portable bioassays, ***Angewandte Chemie-International Edition*** *46*,(8), 1318-1320.
12. A.W. Martinez, S.T. Phillips, E. Carrilho, S.W. Thomas, H. Sindi, and G.M. Whitesides. (2008) Simple telemedicine for developing regions: Camera phones and paper-based microfluidic devices for real-time, off-site diagnosis, ***Analytical Chemistry*** *80*,(10), 3699-3707.
13. E. Carrilho, S.T. Phillips, S.J. Vella, A.W. Martinez, and G.M. Whitesides. (2009) Paper microzone plates, ***Analytical Chemistry*** *81*,(15), 5990-5998.
14. A.W. Martinez, S.T. Phillips, and G.M. Whitesides. (2008) Three-dimensional microfluidic devices fabricated in layered paper and tape, ***Proceedings of the National Academy of Sciences of the United States of America*** *105*,(50), 19606-19611.
15. S.X. Su, M. Ali, C.D.M. Filipe, Y.F. Li, and R. Pelton. (2008) Microgel-based inks for paper-supported biosensing applications, ***Biomacromolecules*** *9*,(3), 935-941.
16. W.A. Zhao, M.M. Ali, S.D. Aguirre, M.A. Brook, and Y.F. Li. (2008) Paper-based bioassays using gold nanoparticle colorimetric probes, ***Analytical Chemistry*** *80*,(22), 8431-8437.
17. J. Wang, R. Pelton, L.J. Veldhuis, C.R. MacKenzie, J.C. Hall, and C.D.M. Filipe.

Wet-strength resins and surface properties affect paper-based antibody assays, ***Appita Journal*** *63*,(1), 32-36.

18. D. Danino, and A. Marmur. (1994) Radial capillary penetration into paper - limited and unlimited liquid reservoirs, ***J. Colloid Interface Sci.*** *166*,(1), 245-250.
19. J.F. Oliver, L. Agbezuge, and K. Woodcock. (1994) A diffusion approach for modeling penetration of aqueous liquids into paper, ***Colloid Surf. A-Physicochem. Eng. Asp.*** *89*,(2-3), 213-226.
20. J. Hyvaluoma, P. Raiskinmaki, A. Jasberg, A. Koponen, M. Kataja, and J. Timonen. (2006) Simulation of liquid penetration in paper, ***Physical Review E*** *73*,(3), 8.
21. P. Aslund. (2004) in Licentiate Thesis:Dynamic measurement of water induced roughening in paper surfaces by a new optical method, Department of Fibre and Polymer Technology, Royal Institute of Technology,Stockholm.
22. R.W. Hoyland, and R. Field. (1976) Review of transudation of water into paper .4. Liquid penetration into paper, ***Paper Technology and Industry*** *17*,(8), 304-306.
23. A. Marmur. (1988) The radial capillary, ***J. Colloid Interface Sci.*** *124*,(1), 301-308.
24. A. Marmur. (1989) Capillary rise in thin porous-media, ***Journal of Physical Chemistry*** *93*,(12), 4873-4877.
25. A. Borhan, and K.K. Rungta. (1993) An experimental-study of the radial penetration of liquids in thin porous substrates, ***J. Colloid Interface Sci.*** *158*,(2), 403-411.
26. D.I. Dimitrov, A. Milchev, and K. Binder. (2007) Capillary rise in nanopores: Molecular dynamics evidence for the lucas-washburn equation, ***Physical Review Letters*** *99*,(5), 4.
27. D.A. Lockington, J.Y. Parlange, and M. Lenkopane. (2007) Capillary absorption in porous sheets and surfaces subject to evaporation, ***Transp. Porous Media*** *68*,(1), 29-36.
28. I.W. Eames, N.J. Marr, and H. Sabir. (1997) The evaporation coefficient of water: A review, ***Int. J. Heat Mass Transf.*** *40*,(12), 2963-2973.
29. N. Fries, K. Odic, M. Conrath, and M. Dreyer. (2008) The effect of evaporation on the wicking of liquids into a metallic weave, ***J. Colloid Interface Sci.*** *321*,(1), 118-129.
30. N. Fries, K. Odic, M. Conrath, M. Dreyer, and Asme. (2008) *The capillary rise of liquids in a metallic weave - evaporation effects*, Amer Soc Mechanical Engineers, New York.
31. C. Kjaergaard, P. Moldrup, L.W. de Jonge, and O.H. Jacobsen. (2004) Colloid mobilization and transport in undisturbed soil columns. Ii. The role of colloid dispersibility and preferential flow, ***Vadose Zone Journal*** *3*,(2), 424-433.
32. J.N. Ryan, and M. Elimelech. (1996) Colloid mobilization and transport in groundwater, ***Colloid Surf. A-Physicochem. Eng. Asp.*** *107*1-56.
33. N.M. DeNovio, J.E. Saiers, and J.N. Ryan. (2004) Colloid movement in unsaturated porous media: Recent advances and future directions, ***Vadose Zone Journal*** *3*,(2), 338-351.
34. T.K. Sen, and K.C. Khilar. (2006) Review on subsurface colloids and colloid-associated contaminant transport in saturated porous media, ***Advances in Colloid and Interface Science*** *119*,(2-3), 71-96.
35. J.P. Herzig, D.M. Leclerc, and P. Goff. (1970) Flow of suspensions through

porous media—application to deep filtration, ***Industrial & Engineering Chemistry*** *62*,(5), 8-35.
36. C. Gruesbeck, and R.E. Collins. (1982) Entrainment and deposition of fine particles in porous-media, ***Society of Petroleum Engineers Journal*** *22*,(6), 847-856.
37. V.B. Pandya, S. Bhuniya, and K.C. Khilar. (1998) Existence of a critical particle concentration in plugging of a packed bed, ***Aiche Journal*** *44*,(4), 978-981.
38. Z. Adamczyk, and P. Weronski. (1999) Application of the dlvo theory for particle deposition problems, ***Advances in Colloid and Interface Science*** *83*,(1-3), 137-226.
39. B. Derjaguin, and L. Landau. (1993) Theory of the stability of strongly charged lyophobic sols and of the adhesion of strongly charged-particles in solutions of electrolytes, ***Prog. Surf. Sci.*** *43*,(1-4), 30-59.
40. G.D. Parfitt, (Ed.) (1981) *Dispersion of powder in liquids with special reference to pigments*, London.
41. S. Patil, J.C. Zhang, K. Tawfiq, and G. Chen. (2009) Role of interfacial interactions in the deposition of colloidal clay particles in porous media, ***Journal of Adhesion Science and Technology*** *23*,(13-14), 1845-1859.
42. J. Zhuang, J. Qi, and Y. Jin. (2005) Retention and transport of amphiphilic colloids under unsaturated flow conditions: Effect of particle size and surface property, ***Environmental Science & Technology*** *39*,(20), 7853-7859.
43. M. Hermansson. (1999) The dlvo theory in microbial adhesion, ***Colloids and Surfaces B-Biointerfaces*** *14*,(1-4), 105-119.
44. D.E. Fontes, A.L. Mills, G.M. Hornberger, and J.S. Herman. (1991) Physical and chemical factors influencing transport of microorganisms through porous-media, ***Applied and Environmental Microbiology*** *57*,(9), 2473-2481.
45. P.A. Deshpande, and D.R. Shonnard. (1999) Modeling the effects of systematic variation in ionic strength on the attachment kinetics of pseudomonas fluorescens uper-1 in saturated sand columns, ***Water Resources Research*** *35*,(5), 1619-1627.
46. E. Rodier, and J. Dodds. (1995) An experimental study of the transport and capture of colloids in a porous medium subjected to step increases in concentration, ***Colloid Surf. A-Physicochem. Eng. Asp.*** *105*,(2-3), 221-231.
47. J. Gannon, Y.H. Tan, P. Baveye, and M. Alexander. (1991) Effect of sodium-chloride on transport of bacteria in a saturated aquifer material, ***Applied and Environmental Microbiology*** *57*,(9), 2497-2501.
48. N. Huber, T. Baumann, and R. Niessner. (2000) Assessment of colloid filtration in natural porous media by filtration theory, ***Environmental Science & Technology*** *34*,(17), 3774-3779.
49. D. Grolimund, M. Elimelech, and M. Borkovec. (2001) Aggregation and deposition kinetics of mobile colloidal particles in natural porous media, ***Colloid Surf. A-Physicochem. Eng. Asp.*** *191*,(1-2), 179-188.
50. P.R. Johnson, and M. Elimelech. (1995) Dynamics of colloid deposition in porous-media - blocking based on random sequential adsorption, ***Langmuir*** *11*,(3), 801-812.
51. T. Dabros, and T.G.M. Vandeven. (1982) Kinetics of coating by colloidal particles, ***J. Colloid Interface Sci.*** *89*,(1), 232-244.
52. M.S. Smith, G.W. Thomas, R.E. White, and D. Ritonga. (1985) Transport of escherichia-coli through intact and disturbed soil columns, ***Journal of Environmental Quality*** *14*,(1), 87-91.
53. F. Huysman, and W. Verstraete. (1993) Water-facilitated transport of bacteria in

unsaturated soil columns - influence of inoculation and irrigation methods, ***Soil Biology & Biochemistry*** *25*,(1), 91-97.
54. M.M. Sharma, H. Chamoun, D. Sarma, and R.S. Schechter. (1992) Factors controlling the hydrodynamic detachment of particles from surfaces, ***J. Colloid Interface Sci.*** *149*,(1), 121-134.
55. A.A.S. Bhagat, S.S. Kuntaegowdanahalli, and I. Papautsky. (2009) Inertial microfluidics for continuous particle filtration and extraction, ***Microfluidics and Nanofluidics*** *7*,(2), 217-226.
56. R. Muller, and D. Clegg. (1951) Paper chromatography-physical and geometric factors, in *Analytical Chemistry*, pp 403-408, Analytical Chemistry.
57. B. Alince, J. Petlicki, and T.G.M. Vandeven. (1991) Kinetics of colloidal particle deposition on pulp fibers .1. Deposition of clay on fibers of opposite charge, ***Colloids and Surfaces*** *59*265-277.
58. B. Alince, M. Inoue, and A.A. Robertson. (1976) Latex-fiber interaction and paper reinforcement, ***J. Appl. Polym. Sci.*** *20*,(8), 2209-2219.
59. B. Alince, A.A. Robertson, and M. Inoue. (1978) Deposition of cationic styrene and styrene-butadiene latex-particles on cellulose fibers, ***J. Colloid Interface Sci.*** *65*,(1), 98-107.
60. B. Alince. (1989) Colloidal particle deposition on pulp fibers, ***Colloids and Surfaces*** *39*,(1-3), 39-51.
61. B. Alince. (1979) Deposition of cationic polymeric pigments on pulp fibers, ***J. Colloid Interface Sci.*** *69*,(3), 367-374.
62. B. Alince, and P. Lepoutre. (1982) Cationic latex in fiber-clay paper composites, ***Journal of Polymer Science Part C-Polymer Letters*** *20*,(12), 615-620.
63. R.D. Deegan, O. Bakajin, T.F. Dupont, G. Huber, S.R. Nagel, and T.A. Witten. (1997) Capillary flow as the cause of ring stains from dried liquid drops, ***Nature*** *389*,(6653), 827-829.
64. S.K. Park, Y.H. Kim, and J.I. Han. (2009) High-resolution patterned nanoparticulate ag electrodes toward all printed organic thin film transistors, ***Organic Electronics*** *10*,(6), 1102-1108.
65. J.X. Huang, A.R. Tao, S. Connor, R.R. He, and P.D. Yang. (2006) A general method for assembling single colloidal particle lines, ***Nano Letters*** *6*,(3), 524-529.
66. R.D. Deegan. (2000) Pattern formation in drying drops, ***Physical Review E*** *61*,(1), 475-485.
67. Y.O. Popov. (2005) Evaporative deposition patterns: Spatial dimensions of the deposit, ***Physical Review E*** *71*,(3), 17.
68. X.Y. Shen, C.M. Ho, and T.S. Wong. Minimal size of coffee ring structure, ***Journal of Physical Chemistry B*** *114*,(16), 5269-5274.
69. C. Seoul, and W.J. Song. (2001) Polymer light-emitting devices based on plasma-polymerized benzene and plasma-polymerized naphthalene, ***Journal of Materials Science-Materials in Electronics*** *12*,(1), 51-55.
70. J. Brant, H. Lecoanet, and M.R. Wiesner. (2005) Aggregation and deposition characteristics of fullerene nanoparticles in aqueous systems, ***Journal of Nanoparticle Research*** *7*,(4-5), 545-553.
71. F. Huysman, and W. Verstraete. (1993) Effect of cell-surface characteristics on the adhesion of bacteria to soil particles, ***Biology and Fertility of Soils*** *16*,(1), 21-26.
72. B.V. Zhmud, F. Tiberg, and K. Hallstensson. (2000) Dynamics of capillary rise, ***J. Colloid Interface Sci.*** *228*,(2), 263-269.

73. S.B. Roy, and D.A. Dzombak. (1996) Colloid release and transport processes in natural and model porous media, ***Colloid Surf. A-Physicochem. Eng. Asp.*** *107*245-262.

74. P.A. Steward, J. Hearn, and M.C. Wilkinson. (2000) An overview of polymer latex film formation and properties, ***Adv. Colloid Interface Sci.*** *86*,(3), 195-267.

75. J.R. Feng, M.A. Winnik, R.R. Shivers, and B. Clubb. (1995) Polymer blend latex films - morphology and transparency, ***Macromolecules*** *28*,(23), 7671-7682.

76. A. Liukkonen. (1997) Contact angle of water on paper components: Sessile drops versus environmental scanning electron microscope measurements, ***Scanning*** *19*,(6), 411-415.

77. R.a.A.-C.E. American Society of Heating. (2003) *Ashrae handbook. Heating, ventilating, and air-conditioning applications.*, American Society of Heating, Refrigerating and Air Conditioning Engineers, Atlanta, GA.